Politecnico di Torino

Master degree programme in Aerospace Engineering

Master degree thesis

Optimal satellite formation reconfiguration based on relative orbital elements

July 2022

Supervisor:
Prof. Lorenzo Casalino

Candidate:
Luca Biddau

Alla mia famiglia, ad Alessia, a Joy, a chi mi è stato vicino durante questi anni

Abstract

The aim of this thesis is to review and further investigate orbital maneuvers on satellite flight formations using relative orbital elements. The study of flight formations applies to twin satellites as well as swarms and constellations of thousands of them, with applications from autonomous rendezvous and docking maneuvers of manned spacecrafts, to Earth and deep space observation through swarms of satellites acting as a virtual radar dish, overcoming the difficulties associated with big, single satellite missions.

After proposing the derivation of the state transition matrices that model the perturbed orbital dynamics, maneuvering schemes found in literature are employed to solve formation reconfiguration problems, highlighting particularly economic or optimal strategies. A new maneuvering strategy is then developed to combine the out-of-plane burns to the in-plane ones, allowing for propellant expense reduction. The relation between orbital elements variations and combined maneuvers' costs are investigated through a series of parametric studies, which find delta-v reductions up to 14.8%.

Contents

Symbols

a	semimajor axis
$\boldsymbol{B}$	control input matrix
e	eccentricity
e_x, e_y	eccentricity vector components
i	inclination
J_2	first zonal harmonic
t	time
u	mean argument of latitude, or mean latitude
$\boldsymbol{u}_T$	vector (collection) of maneuvers' mean latitudes
$\boldsymbol{\alpha}$	vector of classical orbital elements
$\delta\boldsymbol{\alpha}$	vector of relative orbital elements
δa	relative semimajor axis
$\delta\lambda$	relative mean longitude
$\delta\boldsymbol{e}$	relative eccentricity vector
$\delta\boldsymbol{i}$	relative inclination vector
$\delta i_x, \delta i_y$	relative inclination vector components
$\delta\boldsymbol{v}$	velocity impulsive variation in the Hill reference frame
$\Delta\delta\tilde{\boldsymbol{\alpha}}$	effective relative orbital elements change, net of perturbations
θ	true anomaly
ξ	mean argument of latitude difference
φ	relative pericenter
$\boldsymbol{\Phi}_H$	natural dynamics state transistion matrix
$\boldsymbol{\Phi}_{J2}$	perturbed dynamics state transition matrix
ω	argument of periapsis
Ω	right longitude of ascending node

List of Figures

List of Tables

1 Spacecraft Formation Flight

The spacecraft formation flight has been studied since the early sixties, at the beginning of the manned space program, when the challenge was to get two spacecrafts to rendezvous and dock. This was critical for the Apollo space program. In 1969 the US, Soviet Union and European Space Research Organization satellites studied the interaction between solar flares and Earth's magnetic field, achieving the first spatial sampling by a group of separated spacecrafts [1]. In 1978 Antoine Labeyrie proposed in his paper "Stellar interferometry methods" [2] a multi-telescope system in space, free from disturbances present on Earth like microseism and wind. Having multiple satellites flying in a specific geometry avoids the technical and financial challenge of building a radar dish of the equivalent size.

These satellite formations can have diameters up to several kilometers. Attempting to build, control, and navigate a structure that could span such surfaces would be challenging and not cost effective, while having a multitude of satellites form a virtual radar dish avoids many of these issues. The formation flight of satellites today has many other applications, such as positioning systems (like GPS), internet services, cloud observation for better weather forecasting and climate research, Earth observation regarding monitoring of volcanoes, earthquakes and environment pollution, communication and connection to remote and developing areas.

Traditionally these tasks were done by sending large satellites equipped with big payloads and complex on-board systems. Large satellites require big launch vehicles leading to high costs and mission complexity and are more affected by orbital disturbances, requiring bigger correction maneuvers. Besides, in case of failure of one satellite, it is easier to replace one of the spacecrafts during the mission instead of repairing a subsystem of a big spacecraft in space. Modern miniaturization progresses of microprocessors, batteries, actuators, and other hardware parts allow to build smaller satellites able to fly in formation to accomplish the same tasks of bigger, single satellites. A swarm of smaller satellites can offer higher redundancy, and the ability to launch small vehicles as co-passengers of heavier satellites launch, leading to reduced launch costs [3].

Formation flight poses its challenges such as limited propulsion capabilities and batteries capacity, communication between many satellites with limited bandwidth and attitude perturbations. A successful mission that exploits formation flight will then require a precise position and attitude control of the satellites, in order for them to fly with minimum deviations from their intended orbits, despite orbital perturbations such as J2 effect, atmospheric drag, gravity gradient and solar pressure.

Satellite formations can be made of just two spacecrafts called twin satellites, or from hundreds of them. They can be arranged in trailing formations, swarms, or constellations. While in trailing formation they orbit the same path, clusters (or swarms) are groups of satellites moving very close together in almost identical orbits, and in constellations they're typically placed in sets of complementary orbital planes. As an example, the following are completed or in progress missions that count from two to more than 2000 satellites flying in formation, orbiting both Earth and the Moon:

- Gravity Recovery and Climate Experiment (GRACE): carried on by NASA and DLR (German Aerospace Center), it used twin satellites to look for Earth's gravity field anomalies from its launch in March 2002 to the end of the mission in October 2017. By measuring gravity anomalies, GRACE showed how mass is distributed around the planet and how it varies over time. Data from the GRACE satellites is an important tool for studying Earth's ocean, geology, and climate

- Gravity Recovery and Interior Laboratory (GRAIL): carried on by NASA, two small satellites were launched on September 2011 and reached their orbits around the Moon 25 hours apart. By measuring changes in their relative distance as small as one micrometer, the two satellites mapped the gravitational field of the Moon to obtain its geological structure.

- Swarm: ESA's first swarm mission for Earth observation. The mission consists of three identical satellites which were launched on November 2013 into a near-polar orbit. Swarm is dedicated to creating a highly detailed survey of the Earth's geomagnetic field and its temporal evolution as well as the electric field in the atmosphere

Figure 1: Swarm satellites

- Magnetospheric Multiscale Mission MMS: NASA's mission to study Earth's magnetosphere using four identical satellites in a tetrahedral formation, launched on March 2015. In 2016 the mission achieved a new record, with its four spacecraft flying only 7 kilometers apart, the closest separation ever of any formation as reported on NASA's website.

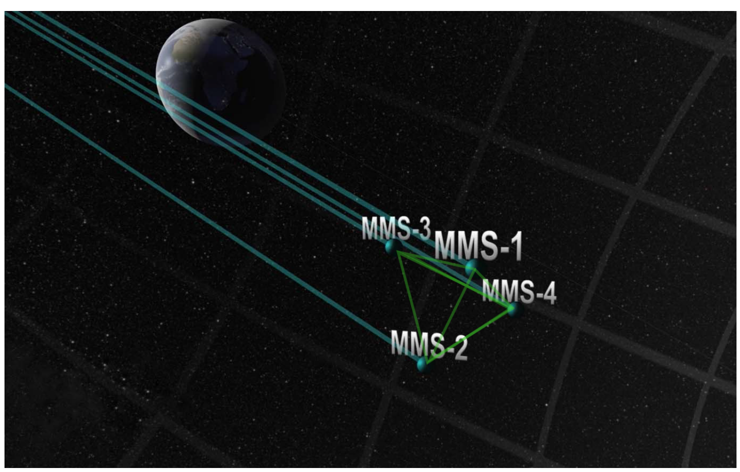

Figure 2: MMS tetrahedral formation

- Starlink: a satellite internet constellation operated by SpaceX, providing satellite Internet access coverage to 33 countries, aiming for global coverage. As of May 2022, Starlink consists of over 2,400 mass-produced small satellites in low Earth orbit which communicate with ground transceivers.

Figure 3: 60 Starlink satellites stacked together before deployment

While the concepts of formation flight apply to the rendezvous and docking maneuvers of spacecraft, the difference with the control of clusters of satellites lies in the different time of flight. Rendezvous and docking maneuvers require little time compared to the lifetime of the vehicle or the missions, and feedback control laws can compensate for orbit modeling errors. Swarms and constellations of satellites are significantly more sensitive to this kind of errors, since formation has to be maintained over the entire life span of the vehicles, which will require more fuel for orbit corrections and can dictate a shorter lifetime of the formation.

Future missions intend to further test formation flight capabilities of small satellites, to achieve relevant scientific goals and perform scientific measurements not possible otherwise, within a small cost. Proba-3 is a technological demonstration mission planned by ESA to observe the Sun corona. It consists of two independent spacecrafts, which will fly close to each other on elliptical orbits up to 60500 km of altitude. The two satellites must be at 150 meters from each other, and maintain this position with accuracy up to the millimeter. Proba-3 will also demonstrate formation flight technologies: station keeping up to 25 meters of distance, approaching and separating in formation, resizing and re-targeting maneuvers [4].

A novel architecture proposed is the Swarms of Silicon Wafer Integrated Femtosatellites (SWIFT), that would enable 100-gram-class spacecraft to be flown as swarms (100s to 1000s) in low Earth orbit, with applications to sparse aperture arrays and distributed sensor networks.The femtosat swarm architecture aims to demonstrate the flexibility and robustness that can be achieved by distributed spacecraft systems [5].

2 Introductory Topics

2.1 The Two Body Problem

The two body problem consists in determining the motion of two bodies due solely to their own mutual gravitational attraction. The two bodies are treated as particles and their rigid body motion is neglected. Assuming that the two masses m_1, m_2 are moving in space, and the position vectors $\boldsymbol{R_1}, \boldsymbol{R_2}$ are measured relative to an inertial reference frame, the position of m_2 relative to m_1 is the vector

$$\boldsymbol{r} = \boldsymbol{R}_2 - \boldsymbol{R_1}$$

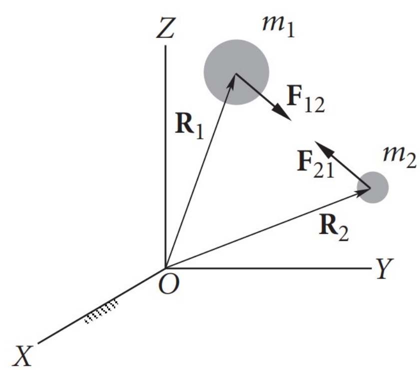

Figure 4: Free body diagram in the inertial reference frame

Using Newton's equation of motion, the inertial equations of motion for each body are written as

$$m_1 \ddot{R}_1 = \frac{G m_1 m_2}{r^3} \boldsymbol{r}$$
$$m_2 \ddot{R}_2 = -\frac{G m_1 m_2}{r^3} \boldsymbol{r}$$

where G is the universal gravity constant. The gravitational coefficient is defined as $\mu = G(m_1 + m_2)$ and can be approximated as $\mu \approx G m_1$ being $m_1 \gg m_2$ true for many systems. By subtracting the two equations of motion:

$$\ddot{\boldsymbol{r}} = -\frac{\mu}{r^3} \boldsymbol{r}$$

This last equation envelops a system of three coupled, nonlinear, scalar differential equations, which decouple only in the particular case of circular orbit. An analytical solution still exists in the most general case. By integrating this equation the fundamental integrals of an orbit are found, one of them being the specific angular momentum vector $\boldsymbol{h} = \boldsymbol{r} \times \dot{\boldsymbol{r}}$, later used to define the orbital parameters. Moreover, it is found that the orbit of the secondary body of mass m_2 around the primary one is a conic section, with body m_1 at the focal point. The equation for the orbit will be, in polar coordinates r, θ:

$$r = \frac{a(1-e^2)}{1+e\cos\theta}$$

where the angle θ is measured from the periapsis in the direction of motion. The semi-major axis a indicates the size of the orbit, and the eccentricity e its flattening. Different values of e correspond to different geometries of the orbit: $e = 0$ will be a circular orbit, $0 < e < 1$ an elliptic orbit, $e = 1$ a parabolic orbit, $e > 1$ a hyperbolic orbit.

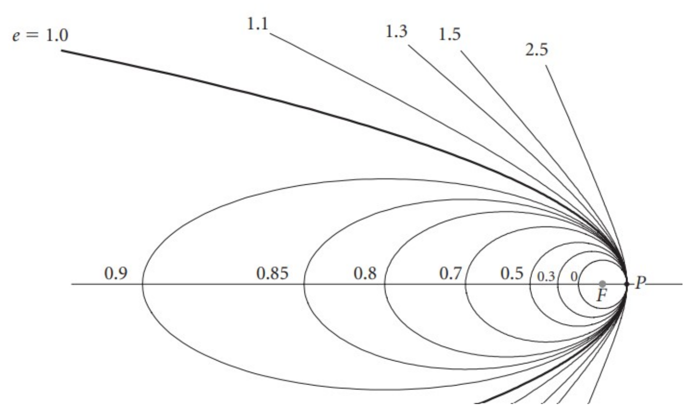

Figure 5: Orbits of various eccentricity, having common focus and periapsis

2.2 Classical orbital elements

[6][7][8]To define the orbital elements it is necessary to introduce the geocentric equatorial reference system. The X axis points in the vernal equinox direction, the XY plane is the Earth's equatorial plane, and the Z axis coincides with the Earth's axis of rotation and

points northward. The unit vectors $\hat{\boldsymbol{I}}, \hat{\boldsymbol{J}}, \hat{\boldsymbol{K}}$ form a right-handed triad. This coordinate systems is not truly inertial, since the center of the Earth is always accelerating towards a third body, but this phenomenon can be ignored in the two-body formulation.

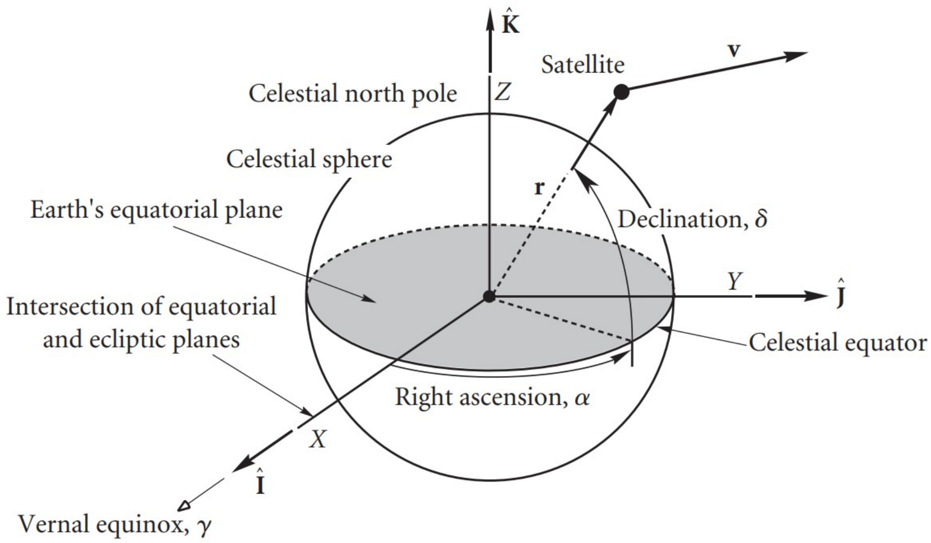

Figure 6: Geocentric equatorial frame

Assuming no orbit perturbations, any two-body orbit geometry can be described through six scalar parameters, called orbital elements. The orbital elements are constant, except for the position of the body within the orbit. A commonly used set of COEs is

$$\boldsymbol{\alpha} = (a, e, i, \Omega, \omega, \theta)$$

The first two elements are the semi-major axis and the eccentricity, which determine the orbit size and shape. The following three scalars are the Euler angles that define the orbit plane orientation in space:

- Inclination i: the angle between the third component of the geocentric-equatorial coordinate system $\hat{\boldsymbol{K}}$ and the angular momentum vector $\boldsymbol{h}$
- Longitude of ascending node Ω: the angle in the equatorial plane measured eastward from the first coordinate axis $\hat{\boldsymbol{I}}$ to

the ascending node, which is the point where the spacecraft crosses the fundamental plane while moving to the northern hemisphere

- Argument of periapsis ω: the angle in the orbit plane between the ascending node and the periapsis, measured in the direction of the spacecraft's motion

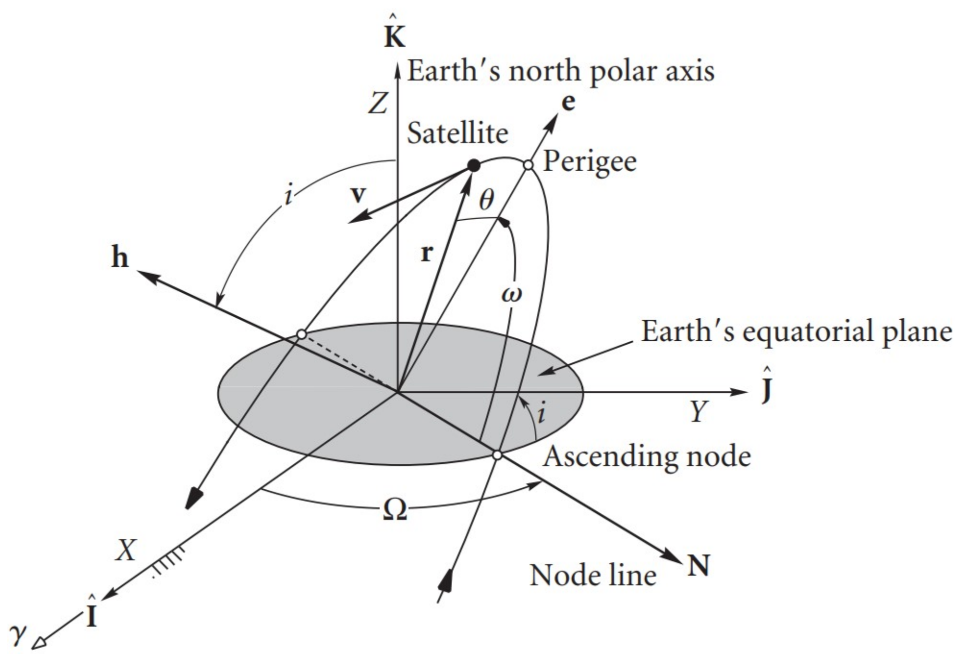

Figure 7: Classical Orbital Elements

Finally, the true anomaly θ specifies where the object is within the orbit at time t, and is measured from the periapsis passage, meaning from the eccentricity vector. The orbital elements can be found from the Cartesian components of the position and velocity vectors $\boldsymbol{r}, \boldsymbol{v}$. First the angular momentum and eccentricity vectors are computed:

$$\boldsymbol{h} = \boldsymbol{r} \times \boldsymbol{v} \quad \boldsymbol{e} = \frac{\boldsymbol{v} \times \boldsymbol{h}}{\mu} - \frac{\boldsymbol{r}}{r}$$

then the following unit vectors:

$$\hat{\boldsymbol{h}} = \frac{\boldsymbol{h}}{h}, \quad \hat{\boldsymbol{r}} = \frac{\boldsymbol{r}}{r}, \quad \hat{\boldsymbol{n}} = \frac{\boldsymbol{N}}{N} = \frac{\hat{\boldsymbol{K}} \times \boldsymbol{h}}{\|\hat{\boldsymbol{K}} \times \boldsymbol{h}\|}, \quad \hat{\boldsymbol{e}} = \frac{\boldsymbol{e}}{e}$$

These vectors are centered in the center of mass of the primary body and define respectively the directions normal to the orbit plane, towards the spacecraft, towards the ascending node, and towards the periapsis. The orbital elements are then given by:

- $e = \|\boldsymbol{e}\|$
- $p = h^2/\mu \longrightarrow a = p/(1-e^2)$
- $\cos i = h_3/h$
- $\cos\Omega = n_1 \quad (\Omega > \pi \quad \text{if} \quad N_2 < 0)$
- $\cos\omega = \hat{\boldsymbol{n}} \cdot \hat{\boldsymbol{e}} \quad (\omega > \pi \quad \text{if} \quad e_3 < 0)$
- $\cos\theta = \hat{\boldsymbol{e}} \cdot \hat{\boldsymbol{r}} \quad (\theta > \pi \quad \text{if } \boldsymbol{r} \cdot \dot{\boldsymbol{r}} < 0)$

The mean anomaly M can be used instead of the true anomaly. These two angles are related by Kepler's equation:

$$E - e\sin E = \sqrt{\frac{\mu}{a^3}}(t - t_0) = M$$

where t_0 is the time of periapsis passage and E is the eccentric anomaly defined as

$$\cos E = \frac{e + \cos\theta}{1 + e\cos\theta}$$

The right quadrant of E is found by knowing that if $0 < \theta < \pi$ then $0 < E < \pi$. The mean anomaly changes by 2π during one orbital revolution, but differently from the true and eccentric anomaly it does it linearly with time. The mean anomaly can then be calculated as $M = M_0 + n(t - t_0)$, where t_0 could also be an arbitrary reference epoch.

When dealing with circular or near-circular orbits it is convenient to use the argument of latitude $u = \theta + \omega$ to express the position of the spacecraft along its orbit, measured from the ascending node to the spacecraft at time t. The argument of latitude can be written in terms of mean anomaly, $u = M + \omega$, called mean argument of latitude.

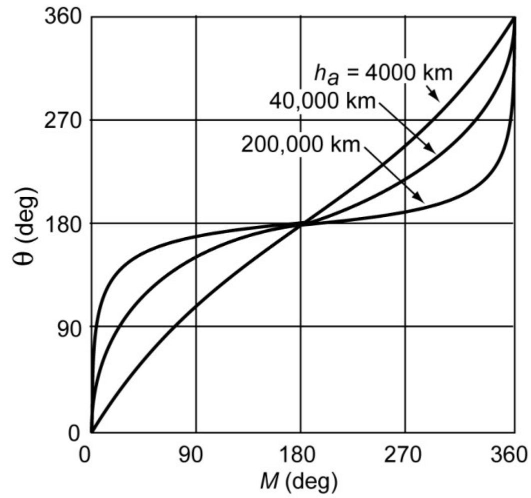

Figure 8: True anomaly as a function of mean anomaly and apoapsis altitude h_a with periapsis altitude $h_p = 400km$

2.3 Effect of Earth's oblateness

[6]The external potential of a perfectly spherical Earth, with an homogeneous mass distribution is described by

$$U = -\frac{\mu}{r}$$

Where r is the distance from Earth's center of gravity. Considering the general case of a body with arbitrary shape, its gravitational potential may be written as

$$U = -\frac{\mu}{r}\left[1 - \sum_{n=2}^{\infty} J_n \left(\frac{R}{r}\right)^n P_n \sin(\varphi) - \sum_{n=2}^{\infty}\sum_{m=2}^{\infty}\left(\frac{R}{r}\right)^n J_{n,m} P_n^m \sin(\varphi)\cos(m\Lambda - \Lambda_{n,m})\right]$$

Where P_n are Legendre's polynomials of degree n, and P_n^m are Legendre's polynomials of degree n and order m, r is the distance from the mass center of the body, φ and Λ are respectively the geocentric latitude and geographic longitude of the generic point. The first term of the perturbed potential represents the gravitational potential of a perfect sphere, while the second term represents the influence of deviations of the shape and mass density distribution in north-south direction (zonal harmonics), and the third term represents the influence of deviations of the shape and mass density distribution in north-south and east-west direction (tesseral and sectorial harmonics). For the tesseral harmonics holds $m \neq n$; for the sectorial harmonics $m = n$.

These effects are larger when the satellite is closer to the Earth. The value of the coefficient of the first perturbing term is $J_2 = 1.083 \cdot 10^{-3}$, while all other J coefficients are three or more orders of magnitude smaller. So the first term produces the largest perturbing force.

A non symmetric gravitational potential will make the orbital

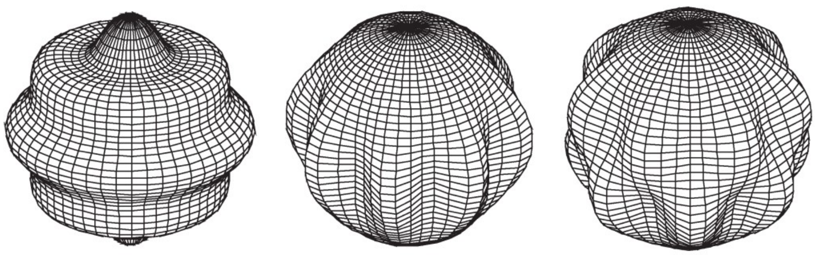

Figure 9: Examples of zonal, sectorial and tesseral harmonics J_{80}, J_{88}, J_{87} on the sphere

elements Ω and ω vary with time. There will be a precession of the node line, and hence, of the orbital plane:

$$\dot{\Omega} = -3\frac{J_2}{2}\frac{R^2}{a^2(1-e^2)^2}n\cos i$$

For prograde orbits the node line will drift westward, since $0 < i < \pi/2$ means $\dot{\Omega} < 0$, this phenomenon is called regression of the nodes. If $\pi/2 < i < \pi$ then $\dot{\Omega} > 0$, so for a retrograde orbit the line of nodes advances eastwards. For polar orbits the node line is stationary. In a similar fashion the argument of periapsis varies as

$$\dot{\omega} = \frac{3}{2}\frac{J_2}{2}\frac{R^2}{a^2(1-e^2)^2}(5\cos^2 i - 1)$$

This expression shows that if $0 < i < 63.4°$ or $116.6° < i < 180°$ then the perigee advances in the direction of the motion of the satellite, otherwise it regresses, moving in the opposite direction. $i = 63.4°$ and $i = 116.6°$ are the critical inclinations at which the apse line does not move.

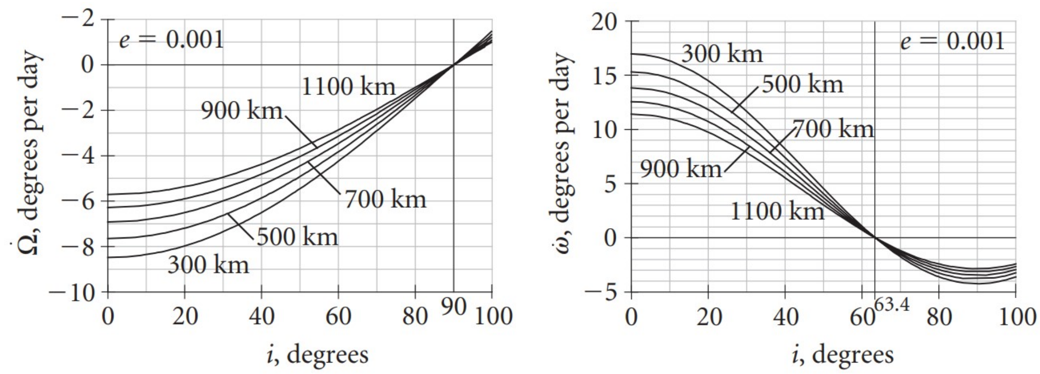

Figure 10: Regression of nodes and advance of apsis for near-circular orbits of altitudes 300 to 1100 km

2.4 Chief-deputy formation

[7]The formation under investigation is composed of a chief and a deputy satellite. The chief satellite is the one about which all other satellite motions are referenced, and it is uncontrolled, or passive. The deputy satellite then flies in formation with the chief, it is controlled by a three dimensional thrust input, also called an active satellite. The relative orbit seen by the chief satellite can be analyzed by introducing the Hill coordinate frame. Its origin is at the chief position, its three axis will constitute a radial-tangential-normal triad $\hat{\boldsymbol{o}}_r, \hat{\boldsymbol{o}}_\theta, \hat{\boldsymbol{o}}_h$. The $\hat{\boldsymbol{o}}_r$ vector will be in the chief's radius direction, $\hat{\boldsymbol{o}}_h$ will be parallel to the orbit's momentum vector, and $\hat{\boldsymbol{o}}_\theta$ completes the right-hand coordinate system. These vectors are defined as:

$$\hat{\boldsymbol{o}}_r = \frac{\boldsymbol{r}_c}{r_c}$$
$$\hat{\boldsymbol{o}}_\theta = \hat{\boldsymbol{o}}_h \times \hat{\boldsymbol{o}}_r$$
$$\hat{\boldsymbol{o}}_h = \frac{\boldsymbol{h}}{h}$$

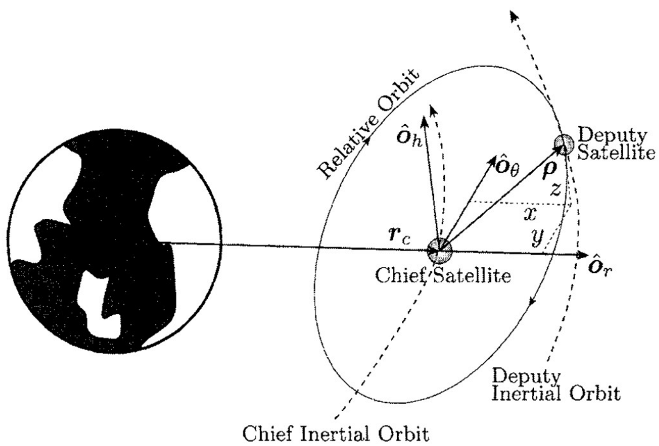

If the chief orbit is circular, then $\hat{\boldsymbol{o}}_\theta$ is parallel to the satellite velocity vector. If the two satellites travel on the same circular orbit, the spacecrafts separation will remain fixed, because the two vehicles are moving at the same orbital speed. If the orbit is elliptic, then the spacecraft separation will contract and expand, depending on whether the formation is approaching the orbit apoapsis or periapsis.

2.5 Relative orbital elements

The set of classical orbital elements is now defined as:

$$\boldsymbol{\alpha} = (a, u, i, \Omega, e_x, e_y)^T$$

where $u = M + \omega$ is the mean argument of latitude, and $\boldsymbol{e}$ is the eccentricity vector, which is useful to avoid singularities in near-circular orbits [9]:

$$\boldsymbol{e} = (e_x, e_y)^T = (e\cos\omega, e\sin\omega)^T$$

A set of relative orbital elements $\delta\boldsymbol{\alpha}$ is then defined as:

$$\delta\boldsymbol{\alpha} = f(\boldsymbol{\alpha}_d, a_c, i_c) - f(\boldsymbol{\alpha}_c, a_c, i_c) = (\delta a, \delta\lambda, \delta i_x, \delta i_y, \delta e_x, \delta e_y)^T$$

Where δa is the relative semi-major axis and $\delta\lambda$ the relative mean longitude. Assuming no perturbations, $\delta\lambda$ is the only time-dependent ROE, which can be written as a function of the mean latitude and δa:

$$\delta\lambda(u) = -\frac{3}{2}(u - u_0)\delta a + \delta\lambda(u_0)$$

The last four components of $\delta\boldsymbol{\alpha}$ constitute the relative eccentricity vector $\delta\boldsymbol{e}$ and relative inclination vector $\delta\boldsymbol{i}$:

$$\delta\boldsymbol{e} = \begin{pmatrix} \delta e_x \\ \delta e_y \end{pmatrix} = \delta e \begin{pmatrix} \cos\varphi \\ \sin\varphi \end{pmatrix}, \quad \delta\boldsymbol{i} = \begin{pmatrix} \delta i_x \\ \delta i_y \end{pmatrix} = \delta i \begin{pmatrix} \cos\theta \\ \sin\theta \end{pmatrix}$$

The angle φ is the relative pericenter, and θ is the argument of latitude at which the deputy spacecraft crosses the orbital plane of the chief spacecraft, defining the relative ascending node N_{12}.

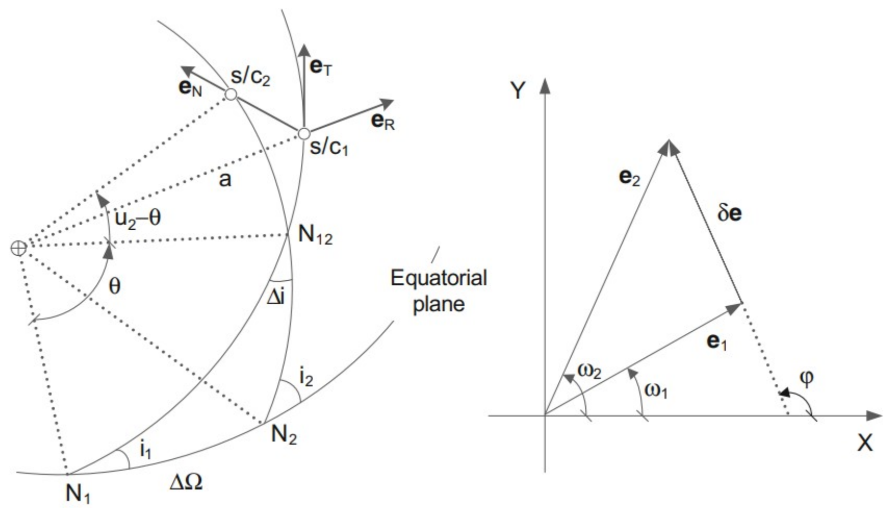

f is a non-linear function of the COEs set $\boldsymbol{\alpha}$:

$$f(\boldsymbol{\alpha}, a_c, i_c) = \begin{pmatrix} a/a_c \\ u + \Omega\cos i_c \\ i \\ \Omega \sin i_c \\ e\cos\omega \\ e\sin\omega \end{pmatrix}$$

so that

$$\delta\boldsymbol{\alpha} = \begin{pmatrix} a_d/a_c - 1 \\ (u_d - u_c) + (\Omega_d - \Omega_c)\cos i_c \\ i_d - i_c \\ (\Omega_d - \Omega_c)\sin i \\ e_d\cos\omega_d - e_c\cos\omega_c \\ e_d\sin\omega_d - e_c\sin\omega_c \end{pmatrix}$$

The relative orbital elements give an insight on the geometry of the two orbits. Both the inclination angle difference and the RAAN differences affects the out-of-plane motion of the deputy spacecraft. δi_x will specify how much out-of-plane motion the relative orbit will have as the satellite flies over high latitude regions, while δi_y shows how much out-of-plane motion there is over equatorial regions [7].

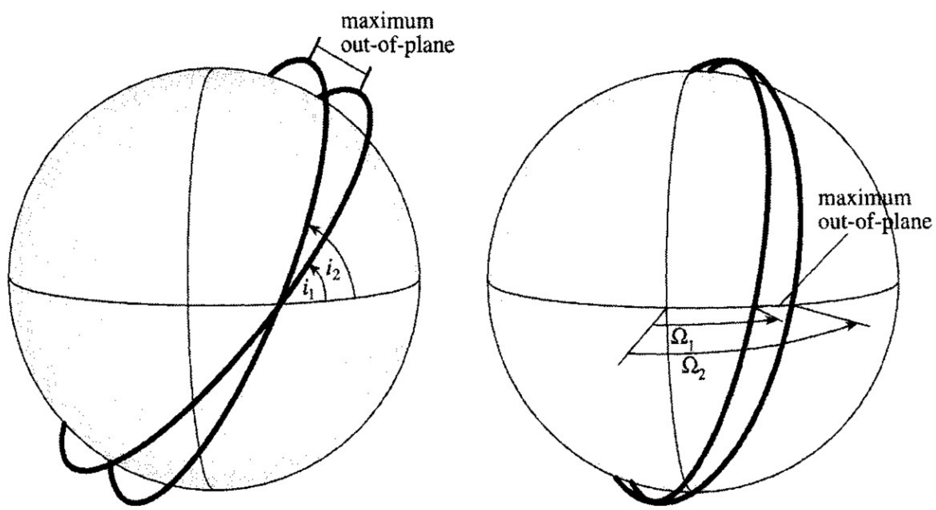

(a) Inclination angle difference (b) Ascending node difference

The relative orbital elements can be linearly mapped to the Cartesian state expressed in the Hill coordinates frame

$$\boldsymbol{x} = \left(x, y, \frac{dx}{dt}, \frac{dy}{dt}, z, \frac{dz}{dt}\right)^T$$

according to $\boldsymbol{x} = \boldsymbol{\mathcal{M}}\delta\boldsymbol{\alpha}$

$$\boldsymbol{\mathcal{M}}(u, n) = \begin{bmatrix} 1 & 0 & -\cos u & -\sin u & 0 & 0 \\ 0 & 1 & 2\sin u & -2\cos u & 0 & 0 \\ 0 & 0 & n\sin u & -n\cos u & 0 & 0 \\ 0 & 0 & 0 & 0 & \sin u & -\cos u \\ 0 & 0 & 0 & 0 & n\cos u & n\sin u \end{bmatrix}$$

The ROE framework has the following peculiarities [10]:

- The availability of a simple and complete closed-form state-transition matrix for the perturbed relative motion, which avoid the need to propagate the orbit by solving differential equations

- The geometrical meaning of each component of the ROEs vector
- The functional structure, later introduced, of the relations between instantaneous velocity variation in the Hill coordinates frame and the effect on the ROEs component
- Distances in the ROE space constitute a metric of the reconfiguration cost.

This last point will be exploited in section 4.6 to understand the numerical results when combining normal and in-plane orbital maneuvers.

3 Model of J_2 perturbed satellite relative motion

3.1 Unperturbed motion

For the Keplerian two-body problem the classical orbital elements are constant, with the exception of the mean argument of latitude u, which varies with a rate of

$$\dot{u} = \sqrt{\frac{\mu}{a^3}} \tag{1}$$

If the two spacecrafts lie on orbits with different semi-major axis, then there will be free drift between them, because of the different rate of variation of u. It is possible to relate δu and δa by taking the differential of Eq.(1) and then considering finite differences: $\Delta(\cdot)$

$$\Delta\dot{u} = -\frac{3}{2}\sqrt{\frac{\mu}{a^3}}\frac{\Delta a}{a} = -\frac{3}{2}n\delta a \tag{2}$$

This relation is valid for Δa smaller than the chief's orbit's radius. By integrating Eq.(11) w.r.t. time:

$$\delta u(t) = -\frac{3}{2}n\delta a\Delta t$$

Where $\Delta t \;\; = t - t_0$. For the unperturbed motion Ω and i are constants, so the mean relative longitude $\delta\lambda$ will vary with time as $\Delta\dot{u}$. It is now possible to write a state transition matrix $\mathbf{\Phi}_H(t, t_0)$ that will map a current state $\delta\boldsymbol{\alpha}_0$ to a new state $\delta\boldsymbol{\alpha}$ according to the unperturbed dynamics:

$$\delta\boldsymbol{\alpha}(t) = \mathbf{\Phi}_H(t, t_0)\delta\boldsymbol{\alpha}_\mathbf{0}$$

$$\mathbf{\Phi}_H(t, t_0) = \begin{bmatrix} 1 & 0 & 0 & 0 & 0 & 0 \\ -\frac{3}{2}n\Delta t & 1 & 0 & 0 & 0 & 0 \\ 0 & 0 & 1 & 0 & 0 & 0 \\ 0 & 0 & 0 & 1 & 0 & 0 \\ 0 & 0 & 0 & 0 & 1 & 0 \\ 0 & 0 & 0 & 0 & 0 & 1 \end{bmatrix}$$

3.2 J_2 perturbed motion

The J_2 effect varies a satellite's COEs according to the following equations [11]:

$$\begin{cases} \dfrac{da}{dt} = \dfrac{de}{dt} = \dfrac{di}{dt} = 0 \\ \dfrac{d\Omega}{dt} = -3\gamma n \cos i \\ \dfrac{d\omega}{dt} = \dfrac{3}{2}\gamma n(5\cos^2 i - 1) \\ \dfrac{dM}{dt} = \dfrac{3}{2}\gamma\eta n(3\cos^2 i - 1) \end{cases} \tag{3}$$

where $\eta = \sqrt{1-e^2}$, $\gamma = \frac{J_2}{2}\frac{R_E^2}{a^2\eta^4}$. To link these equations to the ROEs' time derivatives, every component of $\delta\boldsymbol{\alpha}$ is linearized in the vicinity of the chief orbit as follows:

$$\delta\alpha_i \approx \sum_j \left.\frac{\partial f_i}{\partial \alpha_j}\right|_C \Delta\alpha_j$$

where the index i accounts for the component of f that is being linearized, and j for the COE with respect which we're differentiating. The partial derivatives are evaluated on the COEs of the chief (C) spacecraft. Then $\delta\alpha_i$ is differentiated with respect to time:

$$\frac{d}{dt}(\delta\alpha_i) \approx \sum_j \left.\frac{\partial g_i}{\partial \alpha_j}\right|_C \Delta\alpha_j \tag{4}$$

with $g_i = df_i/dt$.

3.2.1 g_5 derivatives

f_5 is differentiated w.r.t. time:

$$g_5 = \frac{d}{dt}(e\cos\omega) = \cos\omega\frac{de}{dt} + e\frac{d}{dt}(\cos\omega)$$

Since the J_2 effect doesn't alter the orbit's eccentricity the first term of the sum will be zero. The second one is written with Eq.(3) and using $e\sin\omega = e_y$:

$$g_5 = -e\sin\omega\frac{d\omega}{dt} = -\frac{3}{2}\gamma e_y n(5\cos^2 i - 1)$$

Now g_5 is differentiated w.r.t. every COE:

$$\frac{\partial g_5}{\partial a} = -\frac{3}{2}e_y(5\cos^2 i - 1)\frac{\partial}{\partial a}(\gamma n)$$

where

$$\gamma n = \frac{J_2}{2}\frac{R_E^2}{\eta^4}\sqrt{\frac{\mu}{a^7}} \Longrightarrow \frac{\partial}{\partial a}(\gamma n) = -\frac{7}{2}\gamma n\frac{1}{a}$$

thus giving:

$$\frac{\partial g_5}{\partial a} = -\frac{21}{4}e_y(5\cos^2 i - 1)\gamma n\frac{1}{a}$$

Now deriving w.r.t. the eccentricity e:

$$\frac{\partial g_5}{\partial e} = -\frac{3}{2}n\sin(\omega)(5\cos^2 i - 1)\frac{\partial}{\partial e}(\gamma e)$$

$$\frac{\partial}{\partial e}(\gamma e) = \frac{J_2}{2}\frac{R_E^2}{a^2}\frac{\partial}{\partial e}\left(\frac{e}{(1-e^2)^2}\right) = -\gamma\frac{3e^2+1}{1-e^2}$$

And writing the numerator as $4e^2 - e^2 + 1$:

$$\frac{\partial}{\partial e}(\gamma e) = -\gamma\left(1 + 4\left(\frac{e}{\eta}\right)^2\right)$$

Finally:

$$\frac{\partial g_5}{\partial e} = -3\gamma n(5\cos^2 i - 1)\sin\omega\left(\frac{1}{2} + 2\left(\frac{e}{\eta}\right)^2\right)$$

Then g_5 is differentiated w.r.t. to ω and then to i:

$$\frac{\partial g_5}{\partial \omega} = \left(-\frac{3}{2}\gamma en(5\cos^2 i - 1)\right)\frac{\partial}{\partial \omega}\sin\omega = -\frac{3}{2}\gamma e_x n(5\cos^2 i - 1)$$

$$\frac{\partial g_5}{\partial i} = \left(-\frac{3}{2}\gamma en\sin\omega\right)\frac{\partial}{\partial i}(5\cos^2 i - 1) = \frac{15}{2}\gamma n e_y\sin(2i)$$

The function g_5 does not depend by any other classic orbit element. Its time derivative is computed from Eq.(4), where $K = 5\cos^2 i - 1$

$$\frac{d}{dt}\delta e_x = \frac{\partial g_5}{\partial a}(a_d - a_c) + \frac{\partial g_5}{\partial e}(e_d - e_c) + \frac{\partial g_5}{\partial \omega}(\omega_d - \omega_c) + \frac{\partial g_5}{\partial i}(i_d - i_c)$$

By substituting the different derivatives and recognizing the ROEs $\frac{a_d-a_c}{a_d} = \delta a$ and $i_d - i_c = \delta i_x$ we get to:

$$\frac{d}{dt}\delta e_x = \frac{21}{4}\gamma n K e_y \delta a \underbrace{-3\gamma n K\left(\frac{1}{2}+2\left(\frac{e}{\eta}\right)^2\right)(e_d-e_c) - \frac{3}{2}\gamma n K e_x(\omega_d-\omega_c)}_{\aleph} + \frac{15}{2}\gamma n e_y \sin(2i)\delta i_x \tag{5}$$

We look for a time derivative which is function of only ROEs, but this equation still presents some classic orbit elements. An approximation valid for small Δe and $\Delta\omega$ between the two orbits is introduced. The deputy's orbital parameters are written as small increments of the chief ones: $e_d = e_c + \Delta e$ and $\omega_d = \omega_c + \Delta\omega$.

They are substituted in the definition of δe_y, dropping the "c" subscript which is the only last one:

$$\delta e_y \approx (e+\Delta e)\sin(\omega+\Delta\omega) - e\sin(\omega)$$

By using the angle sum identity, the following approximation holds for small values of $\Delta\omega$:

$$\sin(\omega+\Delta\omega) = \sin(\omega)\cos(\Delta\omega)+\cos(\omega)\sin(\Delta\omega) \approx \sin(\omega)+\cos(\omega)\Delta\omega$$

and the second order increment $\Delta e\Delta\omega$ is neglected:

$$\delta e_y \approx e_c\Delta\omega\cos\omega_c + \Delta e\sin\omega_c \tag{6}$$

By operating in the same way we can find an approximation for δe_x:

$$\delta e_x \approx \Delta e\cos\omega_c - e_c\Delta\omega\sin\omega_c \tag{7}$$

These two approximations are then substituted in Eq.(5), where for the sake of clarity $\frac{1}{2}+2\left(\frac{e}{\eta}\right)^2 = f(e)$:

$$\begin{aligned}\aleph &= -3\gamma n K\sin(\omega_c)f(e)(e_d-e_c) - \frac{3}{2}\gamma n K e_x(\omega_d-\omega_c)\\ &= -\gamma n K\left[f(e)\sin(\omega_c)(e_d-e_c)+\frac{1}{2}e_x(\omega_d-\omega_c)\right]\\ &= -3\gamma n K\left[f(e)\sin(\omega_c)\Delta e+\frac{1}{2}e_x\Delta\omega\right]\end{aligned}$$

Since $e_x = e_c\cos\omega_c$ we get:

$$\aleph = -3\gamma n K\left[\frac{1}{2}\sin(\omega_c)\Delta e + \frac{1}{2}e_c\cos(\omega_c)\Delta\omega + 2\left(\frac{e}{\eta}\right)^2\sin(\omega_c)\Delta e\right]$$

By neglecting the first term inside square brackets, because of small Δe, and by using Eq.(6) we finally get to:

$$\aleph \approx -3\gamma n K\left(\frac{1}{2}\delta e_y\right)$$

Which substituted back in Eq.(5) leads us to the result:

$$\boxed{\frac{d}{dt}\delta e_x \approx \frac{21}{4}\gamma n K e_y \delta a - \frac{3}{2}\gamma n K \delta e_y + \frac{15}{2}\gamma n e_y \sin(2i)\delta i_x} \tag{8}$$

3.2.2 g_6 derivatives

The same strategy can be used to find an expression of $d(\delta \dot{e}_y)/dt$. From the definition of g_6:

$$g_6 = \frac{d}{dt}(e\sin\omega) = e\cos(\omega)\frac{d\omega}{dt} = \frac{3}{2}\gamma e n(5\cos^2 i - 1)\cos\omega$$

which gets differentiated w.r.t. the COEs. Using the previous results for $\partial(\gamma n)/\partial a$ and $\partial(\gamma e)/\partial e$ we get:

$$\begin{aligned}
\frac{\partial g_6}{\partial a} &= -\frac{21}{4}\gamma n e_x(5\cos^2 i - 1)\frac{1}{a} \\
\frac{\partial g_6}{\partial e} &= 3\gamma n\cos(\omega)(5\cos^2 i - 1)f(e_c) \\
\frac{\partial g_6}{\partial \omega} &= -\frac{3}{2}\gamma e_y n(5\cos^2 i - 1) \\
\frac{\partial g_6}{\partial i} &= -\frac{15}{2}\gamma n e_x \sin(2i)
\end{aligned}$$

The time derivative of δe_y is written with Eq.(4):

$$\frac{d}{dt}(\delta e_y) \approx -\frac{21}{4}\gamma n e_x K\delta a + \underbrace{3\gamma n\cos(\omega)Kf(e)(e_d - e_c) - \frac{3}{2}\gamma e_y n K(\omega_d - \omega_c)}_{\beth} - \frac{15}{2}\gamma n e_x \sin(2i)\delta i_x$$

Writing once again e_d and ω_d as small increments of e_c and ω_c we can get to the following expression:

$$\beth = 3\gamma n K\left(\frac{1}{2}\cos(\omega)\Delta e - \frac{1}{2}e_c\sin(\omega_c)\Delta\omega + 2\cos(\omega)\left(\frac{e}{\eta}\right)^2\Delta e\right)$$

Neglecting the term which depends from $(\frac{e}{\eta})^2\Delta e$ and using Eq.(6):

$$\beth \approx 3\gamma n K \left(\frac{1}{2}\delta e_x\right)$$

and finally:

$$\boxed{\frac{d}{dt}\delta e_y = -\frac{21}{4}\gamma n e_x K \delta a + \frac{3}{2}\gamma n K \delta e_x - \frac{15}{2}\gamma n e_x \sin(2i)\delta i_x} \tag{9}$$

3.2.3 Integrating g_5 and g_6

Equations (8) and (9) link the time derivatives of δe_x and δe_y to these functions themselves, that are functions of time because are affected by the J_2 effect. These two first order differential equations can be integrated as a system of ODEs. Eq.(8) and Eq.(9) can be further simplified by neglecting the terms dependent on $\delta\alpha$ or δi, which is possible with the assumption of small eccentricity e of the chief's orbit.

Then, since the coefficient in front of both δe_x and δe_y is the derivative of the relative perigee w.r.t. the mean latitude

$$\frac{3}{2}\gamma K = \frac{d\varphi}{du} = \varphi'$$

the following system of differential equations can be written:

$$\begin{cases} \dfrac{d}{dt}(\delta e_x) = -\varphi' n \delta e_y \\ \dfrac{d}{dt}(\delta e_y) = \varphi' n \delta e_x \end{cases}$$

and by differentiating each equation w.r.t. time we get to two second-order differential equations with known analytical solutions:

$$\begin{cases} \dfrac{d^2}{dt^2}(\delta e_x) + (\varphi' n)\delta e_x = 0 \\ \dfrac{d^2}{dt^2}(\delta e_y) + (\varphi' n)\delta e_y = 0 \end{cases} \longrightarrow \boxed{\begin{cases} \delta e_x = \delta e_{x0}\cos(\varphi'\Delta t) - \delta e_{y0}\sin(\varphi'\Delta t) \\ \delta e_y = \delta e_{y0}\cos(\varphi'\Delta t) + \delta e_{x0}\sin(\varphi'\Delta t) \end{cases}}$$

3.2.4 g_4 derivatives

f_4 has to be derived w.r.t. time:

$$g_4 = \frac{d}{dt}f_4 = \frac{d\Omega}{dt}\sin i_c = -3\gamma n \cos i \sin i_c$$

then differentiated w.r.t. a,e and i, where $\partial\gamma/\partial e = 4\gamma e/\eta^2$:

$$\frac{\partial g_4}{\partial a} = \frac{21}{2}\gamma n \frac{1}{a}\cos i \sin i_c$$

$$\frac{\partial g_4}{\partial e} = -12\gamma n \cos i \sin i_c \left(\frac{e}{\eta^2}\right)$$

$$\frac{\partial g_4}{\partial i} = 3\gamma n \sin i \sin i_c$$

The derivatives are summed according to Eq.(4), using $\frac{a_d - a_c}{a_c} = \delta a$, $i_d - i_c = \delta i$, and $\sin(i_c)\cos(i_c) = \sin(2i_c)/2$:

$$\frac{d}{dt}\delta i_y = \frac{21}{4}\gamma n \sin(2i_c)\delta a + 3\gamma n \sin^2(i_c)\delta i_x - 6\gamma n \sin(2i_c)(e_d - e_c)\frac{e_c}{\eta^2}$$

For near-circular orbits $e \approx 0$, which also means $\eta \approx 1$, so the last term in the sum can be neglected:

$$\boxed{\frac{d}{dt}\delta i_y = \frac{21}{4}\gamma n \sin(2i_c)\delta a + 3\gamma n \sin^2(i_c)\delta i_x} \tag{10}$$

3.2.5 g_2 derivatives

The second component of $\delta\boldsymbol{\alpha}$ is $f_2 = u + \Omega\cos i_c$. First $\tilde{g}_2 = du/dt$ is differentiated w.r.t. every COE, then a change of variables is performed, in order to get an expression for $d(\delta\lambda)/dt$. Using $\delta\lambda$ instead of δu will decouple the in-plane and out-of-plane motion.

$$\tilde{g}_2 = \frac{du}{dt} = \frac{df_2}{dt} - \Omega\cos i_c$$

Where the mean argument of latitude is defined as $u = M + \omega$. To compute its time derivative Eq(3) is used:

$$\frac{du}{dt} = \frac{d}{dt}(M + \omega) = \frac{3}{2}\gamma n(K + \eta H)$$

Where $H = 3\cos^2 i - 1$ is a constant. $\tilde{g}_2$ can now be differentiated w.r.t. the COEs:

$$\frac{\partial\tilde{g}_2}{\partial a} = \frac{3}{2}(K + \eta H)\frac{\partial}{\partial a}(\gamma n) = -\frac{21}{4}\gamma n\frac{1}{a}(K + \eta H)$$

$$\frac{\partial \tilde{g}_2}{\partial e} = \frac{\partial}{\partial e}\left(\frac{3}{2}\frac{J_2}{2}\frac{R_E^2}{a^2}\frac{1}{(1-e^2)^2}(K+\sqrt{1-e^2}H)\right) = 3\gamma n e\left(\frac{2}{\eta^2}K + \frac{3}{2}\frac{H}{\eta}\right)$$

$$\frac{\partial \tilde{g}_2}{\partial i} = -\frac{3}{2}\gamma n \sin(2i)(5+3\eta)$$

The derivatives can now be combined according to Eq.(4):

$$\frac{d}{dt}(\delta u) = -\frac{21}{4}\gamma n(K+\eta H)\delta a + 3\gamma n e_c\left(\frac{2}{\eta^2}K + \frac{3}{2\eta}H\right)(e_d - e_c) + \\ -\frac{3}{2}\gamma n \sin(2i)(5+3\eta)\delta i_x \tag{11}$$

Using the approximations Eq.(7) and Eq.(6) it can be shown that the coefficient $e_c(e_d - e_c)$ in the second term of the sum is equal to $e_x\delta e_x + e_y\delta e_y$:

$$\begin{aligned} e_x\delta e_x + e_y\delta e_y &= e\cos\omega(\cos\omega\Delta e - e\sin\omega\Delta\omega) + e\sin\omega(\sin\omega\Delta e + e\cos\omega\Delta e) \\ &= e\cos^2\omega\Delta e - e^2\sin\omega\cos\omega\Delta\omega + e\sin^2\omega\Delta e + e^2\sin\omega\cos\omega\Delta\omega \\ &\approx e\Delta e(\sin^2\omega + \cos^2\omega) = e\Delta e = e_c(e_d - e_c) \end{aligned}$$

Where the terms dependent on e^2 have been neglected, because of the near-circular orbits hypothesis. Thus the second term of Eq.(11) is the only one dependent on e, since $e_x\delta e_x = e_c\cos\omega(e_d - e_c) \propto e^2$, and it can be neglected:

$$\frac{d}{dt}(\delta u) = -\frac{21}{4}\gamma n(K+\eta H)\delta a - \frac{3}{2}\gamma n\sin(2i)(5+3\eta)\delta i_x$$

The mean relative longitude - mean relative latitude relation $\delta u = \delta\lambda - \delta i_y \cot i_c$ is now differentiated to get:

$$\frac{d}{dt}(\delta\lambda) = \frac{d}{dt}(\delta u) + \cot(i_c)\frac{d}{dt}\delta(\delta i_y)$$

By substituting in this last equation the expressions for $d(\delta u)/dt$ and Eq.(10), and by factoring out the ROEs we get:

$$\frac{d}{dt}(\delta\lambda) = \frac{21}{4}\left[-\gamma n(K+\eta H) + \cot(i_c)\gamma n\sin(2i)\right]\delta a + \left[-\frac{3}{2}\gamma n\sin(2i)(3\eta+5) + 3\cot(i_c)\gamma n\sin^2(i)\right]\delta i_x$$

The first term in square brackets is equal to $-\frac{21}{4}\gamma n[H(\eta+1)]$, while the second one can be simplified using the identity $\cot(i_c)\sin^2(i_c) =$

$\sin(2i_c)/2$, leading to $-\frac{3}{2}\gamma n \sin(2i_c)(3\eta+4)$. The resulting equation is:

$$\boxed{\frac{d}{dt}(\delta\lambda) = \frac{21}{4}\gamma n[H(\eta+1)]\delta a + \frac{3}{2}\gamma n \sin(2i_c)(3\eta+4)\delta i_x} \tag{12}$$

3.2.6 $\mathbf{\Phi}_{J2}$ Matrix

Equations (10) and (12) can be easily integrated w.r.t. time, since their right hand sides are not functions of t. It is then possible to arrange all the developed equations in a matrix $\mathbf{\Phi}_J(t,t_0)$, which is summed to $\mathbf{\Phi}_H(t,t_0)$:

$$\mathbf{\Phi}_J(t,t_0) = \begin{bmatrix} 0 & 0 & 0 & 0 & 0 & 0 \\ -\frac{21}{4}\gamma H(\eta+1)\Delta t & 0 & -\frac{3}{2}\gamma\sin(2i)(3\eta+4)\Delta t & 0 & 0 & 0 \\ 0 & 0 & 0 & 0 & 0 & 0 \\ \frac{21}{4}\gamma\sin(2i)\Delta t & 0 & 3\gamma\sin^2(i)\Delta t & 0 & 0 & 0 \\ 0 & 0 & 0 & 0 & \cos(\varphi'\Delta t) & -\sin(\varphi'\Delta t) \\ 0 & 0 & 0 & 0 & \sin(\varphi'\Delta t) & \cos(\varphi'\Delta t) \end{bmatrix} \tag{13}$$

$$\mathbf{\Phi}(t,t_0) = \mathbf{\Phi}_H(t,t_0) + \mathbf{\Phi}_J(t,t_0)$$

and $\mathbf{\Phi}(t,t_0)$ maps a current state $\boldsymbol{\delta}\alpha_0$ in a future state $\boldsymbol{\delta}\alpha$.

$$\delta\boldsymbol{\alpha}(t) = \mathbf{\Phi}(t,t_0)\delta\boldsymbol{\alpha_0} \tag{14}$$

From now on, the state transition matrix will be written as $\mathbf{\Phi}(t_1,t_0) = \mathbf{\Phi}_{1,0}$. Moreover, the following identity is true: $\mathbf{\Phi}_{2,1}\cdot\mathbf{\Phi}_{1,0} = \mathbf{\Phi}_{2,0}$

4 Orbital maneuvers computation and formation reconfiguration

4.1 Orbital maneuvers computation

An impulsive maneuver at the mean argument of latitude u_M produces the following ROEs variations:

$$\begin{pmatrix} \Delta\delta a \\ \Delta\delta\lambda \\ \Delta\delta i_x \\ \Delta\delta i_y \\ \Delta\delta e_x \\ \Delta\delta e_y \end{pmatrix} = \frac{1}{na} \begin{bmatrix} 0 & 2 & 0 \\ -2 & 0 & 0 \\ 0 & 0 & \cos u_M \\ 0 & 0 & \sin u_M \\ \sin u_M & 2\cos u_M & 0 \\ -\cos u_M & 2\sin u_M & 0 \end{bmatrix} \begin{pmatrix} \delta v_R \\ \delta v_T \\ \delta v_N \end{pmatrix}$$

$$\Delta\delta\boldsymbol{\alpha} = \boldsymbol{B}(u_M)\delta\boldsymbol{v} \tag{15}$$

Some considerations about these equations [12]:

- There are two possible ways to establish a $\delta\lambda$ variations: through the natural dynamics of the system along a certain time span, or through a radial delta-v
- δa and $\delta\boldsymbol{e}$ are both varied by tangential burns, with $\Delta\delta\boldsymbol{e}$ depending on the maneuvers' locations u_M. Thus there are values of u_M that reduce the required delta-v
- $\delta\boldsymbol{e}$ can be varied by pure radial or tangential burns. The tangential maneuvers will require half the delta-v of the radial ones.
- Tangential burns allow to change all in-plane ROEs: δa and $\delta\boldsymbol{e}$ are directly changed, while $\delta\lambda$ will vary with time.

When j maneuvers have to be performed, the initial state $\delta\boldsymbol{\alpha}_0$ will meet the final one $\delta\boldsymbol{\alpha}_F$ as follows, according to Eq.(14) and Eq.(15)

$$\begin{aligned} \delta\boldsymbol{\alpha}_1 &= \Phi_{1,0}\delta\boldsymbol{\alpha}_0 + \boldsymbol{B}_1\delta v_1 \\ \delta\boldsymbol{\alpha}_2 &= \boldsymbol{\Phi}_{2,1}\delta\boldsymbol{\alpha}_1 + \boldsymbol{B}_2\delta\boldsymbol{v}_2 = \boldsymbol{\Phi}_{2,0}\delta\boldsymbol{\alpha}_0 + \boldsymbol{\Phi}_{2,1}\boldsymbol{B}_1\delta v_1 + \boldsymbol{B}_2\delta\boldsymbol{v}_2 \\ &\vdots \\ \delta\boldsymbol{\alpha}_j &= \boldsymbol{\Phi}_{F,j}\delta\boldsymbol{\alpha}_j + \boldsymbol{B}_j\delta\boldsymbol{v}_j \end{aligned}$$

Then, the reconfiguration $\delta\boldsymbol{\alpha}_0 \longrightarrow \delta\boldsymbol{\alpha}_F$ can be written as

$$[\boldsymbol{\Phi}_{F,1}\boldsymbol{B}_1, \ldots, \boldsymbol{\Phi}_{F,j}\boldsymbol{B}_j]\delta\boldsymbol{v} = \delta\boldsymbol{\alpha}_F - \boldsymbol{\Phi}_{F,0}\delta\boldsymbol{\alpha}_0$$
$$\boldsymbol{M}\delta\boldsymbol{v} = \Delta\delta\tilde{\boldsymbol{\alpha}}$$

4.2 In-plane reconfiguration with two maneuvers

[12]The two maneuvers solution can establish not more than three ROEs through a pair of tangential-radial burns. The δv values are found solving the in-plane reconfiguration problem:

$$\boldsymbol{M}(u_F, u_1, \xi)\delta\boldsymbol{v} = \Delta\delta\tilde{\boldsymbol{\alpha}}|_{ip} \tag{16}$$

where $\boldsymbol{M}$ is the following 4×4 matrix, derived from the equations of ROEs variations:

$$\boldsymbol{M} = \begin{bmatrix} 0 & 2 & 0 & 2 \\ -2 & -3(u_F - u_1) & 2 & -3(u_F - (u_1 + \xi)) \\ \sin u_1 & 2\sin u_1 & \sin(u_1 + \xi) & 2\cos(u_1 + \xi) \\ -\cos u_1 & 2\cos u_1 & -\cos(u_1 + \xi) & 2\sin(u_1 + \xi) \end{bmatrix}$$

$\delta\boldsymbol{v}$ is the following vector:

$$\delta\boldsymbol{v} = (\delta v_{R1}, \delta v_{T1}, \delta v_{R2}, \delta v_{T2}) = (x_1, x_2, x_3, x_4)^T$$

and $\Delta\delta\tilde{\boldsymbol{\alpha}}|_{ip}$ represents the in-plane components of the vector of variation of ROEs:

$$\Delta\delta\tilde{\boldsymbol{\alpha}} = (\Delta\delta\tilde{a}, \Delta\delta\tilde{\lambda}, \Delta\delta\tilde{e}_x, \Delta\delta\tilde{e}_y)^T = (A, L, E, F)^T$$

While treating the in-plane reconfigurations it will be used the notation $\Delta\delta\tilde{\boldsymbol{\alpha}}$ for the sake of clarity.

Solution №3 employs only tangential burns, and can achieve a reconfiguration only when a correction of the relative semi-major axis is needed ($A \neq 0$). u_1 and ξ are computed numerically, by minimizing the cost function $J = \delta\boldsymbol{v}^T\delta\boldsymbol{v}$, where the delta-v expression is found analytically as $\delta\boldsymbol{v} = \boldsymbol{M}^{-1}\Delta\delta\tilde{\boldsymbol{\alpha}}$. The δv values are then computed from the expressions derived from Eq.(16) with $x_1 = x_3 = 0$:

$$\begin{cases} x_2 = -\frac{3A(u_F - \xi - u_1) + 2L}{6\xi} \\ x_4 = -\frac{3A(u_F - u_1) + 2L}{6\xi} \end{cases}$$

Solution №8 regards a pure radial maneuver ($x_2 = x_4 = 0$) where $\Delta\delta a$ and $\Delta\delta\lambda$ are zero. The optimal, double pulse, radial maneuver is distinguished by $\xi = \pi$. The first burn is located at an angle

$$u_1 = \hat{u} + k\pi \qquad \hat{u} = \arctan\left(-\frac{E}{F}\right)$$

with k being an odd integer. The delta-v vector is then written as

$$\delta\boldsymbol{v} = \frac{1}{2}\|\delta\boldsymbol{e}\|(g, -g)^T$$

Using the following expression for the variation of the relative eccentricity vector component:

$$a\Delta\delta e_x = \frac{1}{n}\delta v_r \sin u_1 \tag{17}$$

and given that that $\sin u_2 = \sin(u_1 + \pi) = -\sin u_1$, it follows that in order to achieve a non-null relative eccentricity variation the two burns must have different signs. The sign of the first pulse can be determined from Eq.(17):

$$\mathrm{sgn}(\delta v_{r1}) = \mathrm{sgn}(x_2) = g = \frac{\mathrm{sgn}(E)}{\mathrm{sgn}(\sin u_1)}$$

The value of g is correct regarding the sign of $\Delta\delta e_y$ as well, given the following equation for its variation, and the different values of u_1 as a function of E and F:

$$a\Delta\delta e_y = -\frac{1}{n}\delta v_R \cos u_M$$

$$u_1 = \arctan\left(-\frac{E}{F}\right) + k\pi \implies \begin{cases} u_1 \in (\frac{\pi}{2}, \pi) & \text{if } \mathrm{sgn}(E) = \mathrm{sgn}(F) \\ u_1 \in (\pi, \frac{3}{2}\pi) & \text{if } \mathrm{sgn}(E) \neq \mathrm{sgn}(F) \end{cases}$$

where $k = 1$ has been chosen.

Solution №9 regards a more general case where $\Delta\delta a \vee \Delta\delta\lambda$ are not null. The pulses will have both radial and tangential components, spaced once again by $\xi = \pi$. The cost function J will be a transcendental function of u_1, which will be found by minimizing J numerically.

Solution №10 regards reconfigurations with only relative eccentricity variations. The radial-tangential pulses latitudes u_1, u_2 are not spaced by π anymore; both are found by minimizing J numerically.

Solution №11 is the most general case, where any ROE can be established and u_1, ξ are found by minimizing J numerically. In №9,№10 and №11 $\delta\boldsymbol{v}$ components are then computed by Eq.(16)

4.3 In-plane reconfigurations with three maneuvers

[12]Considering three impulsive in-plane maneuvers, the reconfiguration problem is written as

$$\boldsymbol{M}(u_F, u_1, u_2, u_3)\delta\boldsymbol{v} = \Delta\delta\tilde{\boldsymbol{a}} \tag{18}$$

where $\delta\boldsymbol{v} = (x_1, x_2, x_3, x_4, x_5, x_6)^T$. We consider only tangential maneuvers by imposes $x_1 = x_3 = x_5 = 0$. The number of unknowns is now six.

Solution №12 considers maneuvers that occur at multiples of half the orbital period of the following mean latitude:

$$\bar{u} = \arctan\left(\frac{F}{E}\right)$$

which is the phase of the total variation of the relative eccentricity vector $\delta\boldsymbol{e}$. The maneuvers' latitudes will then be $u_i = \bar{u} + k_i\pi$, with k_i being an odd integer. This spacing is a necessary condition of the minimization of the total delta-v. The optimal coefficients set (k_1, k_2, k_3) can be found by solving Eq.(18) for every admissible combination of k_i coefficients (such that $k_1 < k_2 < k_3$ and $u_3 \leq u_F$), and picking the one the minimizes the sum $\delta v_{tot} = |x_2| + |x_4| + |x_6|$.

Solution №13 imposes a constraint on the first and third impulses' locations $u_1 = u_0$ and $u_3 = u_F$, reducing the number of unknowns to four and allowing to exploit the whole transfer time to achieve the reconfiguration. u_2 is found by solving numerically the following equation

$$f(u_2) = u_2 - \tilde{K}\cos u_2 - \tilde{P}\sin u_2 - \tilde{Q} = 0$$

where

$$\tilde{D} = 3\cos(u_0)(A\sin(u_F) - F) - 3E\sin(u_F) + \sin(u_0)[3E - 3A\cos(u_F) + 3F\cos(u_F)]$$

$$\tilde{K} = -[3u_0(F - A\sin(u_F)) + 3Au_F\sin(u_F) + 2L\sin(u_F) - 3Fu_F - 2L\sin(u_0)]/\tilde{D}$$
$$\tilde{P} = -[3u_0(A\cos(u_F) - 3E) - 3Au_F\cos(u_F) - 2L\cos(u_F) + 3Eu_F + 2L\cos(u_0)]/\tilde{D}$$
$$\begin{aligned}\tilde{Q} = &- [\cos(u_0)(-3Au_F\sin(u_F) - 2L\sin(u_F) + 3Fu_F) + 3u_0(E\sin(u_F) + \\ &- F\cos(u_F)) + \sin(u_0)(3Au_F\cos(u_F) + 2L\cos(u_F) - 3Eu_F)]/\tilde{D}\end{aligned}$$

For values of $|\tilde{Q}|$ sufficiently small, $f(u_2)$ has more than one zero, leading to different (u_0, u_2, u_F) solutions, with different total delta-v costs. The admissible solution has to satisfy $u_0 < u_2 < u_F$. It is then possible to solve Eq.(3) for every set of mean latitudes and pick the one that minimizes δv_{tot}.

Number of $\delta\boldsymbol{v}$s	₦	$\delta\boldsymbol{v}$ direction	$\delta\boldsymbol{v}$ Locations (u_1, ξ)	Conditions on $\Delta\delta\tilde{\boldsymbol{\alpha}}$
Two pulses	3	T-T	u_1, ξ	$A \neq 0$
	8	R-R	$\hat{u} + \pi, \pi$	$A = L = 0$
	9	RT-RT	u_1, π	-
	10	RT-RT	u_1, ξ	$A = L = 0$
	11	RT-RT	u_1, ξ	-
Three pulses	12	T-T-T	$\bar{u} + k_i\pi$	-
	13	T-T-T	u_0, u_2, u_F	-

4.4 In-plane reconfiguration: numerical results

This section presents the results of the simulations of two different reconfigurations. Both of them have the same starting ROEs vector $\delta\boldsymbol{\alpha}_0$ and a different final aimed state $\delta\boldsymbol{\alpha}_F$. E1 represents a reconfiguration between two bounded orbits, where only the relative eccentricity vector needs to be varied. E2 requires a relative semi-major axis and relative mean longitude variation as well, but the dominant correction is needed on $\delta\boldsymbol{e}$.

The chief spacecraft orbit is circular at 750 km altitude, with an inclination $i = 63.4°$. The reconfiguration has to occur in 2.5 orbital periods, starting with the deputy satellite at the ascending node, meaning $u_0 = 0$ and $u_F = 5\pi$.

4.4.1 Problem E1

The next table uses $a\delta\boldsymbol{\alpha} = a(\delta a, \delta\lambda, \delta e_x, \delta e_y)^T$, since the out of plane dynamic is not considered:

E1

$a\delta\boldsymbol{\alpha}_0$ $[m]$				$a\delta\boldsymbol{\alpha}_F$ $[m]$			
0	-10000	200	-10	0	-10000	230	50

₦	u_1	u_2	u_3	δv_{R1}	δv_{T1}	δv_{R2}	δv_{T2}	δv_{R3}	δv_{T3}	δv_{tot}
-		rad					m/s			
8	2.6885	5.8301	-	0.0361	0	-0.0361	0	-	-	0.0722
10	0.0871	5.2899	-	-0.0322	0.0083	-0.0322	-0.0083	-	-	0.0665
12	4.2487	7.3903	10.5319	0	-0.009	0	0.0181	0	-0.009	0.0361
13	0	4.6356	15.7080	0	0.0231	0	-0.0327	0	0.0098	0.0656

Table 2: Problem E1 and solutions

Solution ₦12 achieves the final state with the lowest total delta-v, which matches the delta-v lower bound. The lower bound LB is a function of the aimed ROEs variation and can be written as follows:

$$LB = \max\left\{\frac{na}{2}\|\Delta\delta\boldsymbol{e}\|, \frac{na}{2}\Delta\delta a^*\right\}$$

where:

$$\Delta\delta a^* = \max\{|\delta a_F - \delta a_0|, |\delta a^*_{transf} - \delta a_0|, |\delta a^*_{transf} - \delta a_F|\}$$

with $\delta a^*_{transf} = 2\Delta\delta\lambda/3\Delta u$ being the minimum relative semi-major axis for accomplishing a given $\delta\lambda$ variation over the $\Delta u = u_F - u_0$ mission's mean latitudes span. Figure 11 shows the relative orbits in the tangential-radial plane obtained from solutions in Table 1.

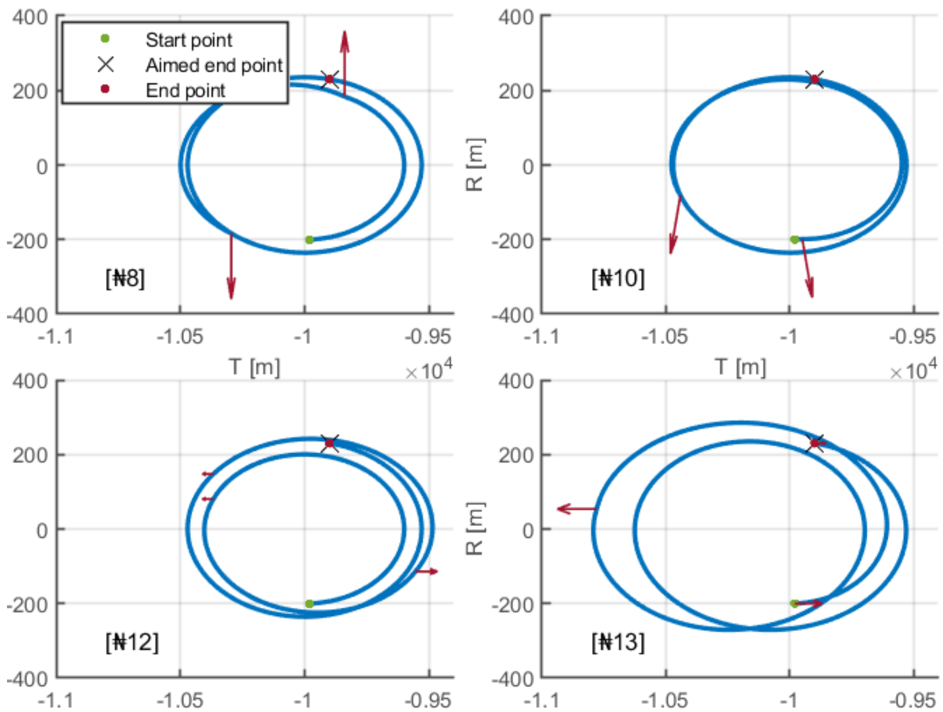

Figure 11: Relative orbits in reconfiguration E1, tangential-radial plane

The following plots show the cost function $J(u_1, \xi)$ as a function of one of its variables when the other one is fixed at its optimal value, set from the function minimization. The red circle shows these optimal values.

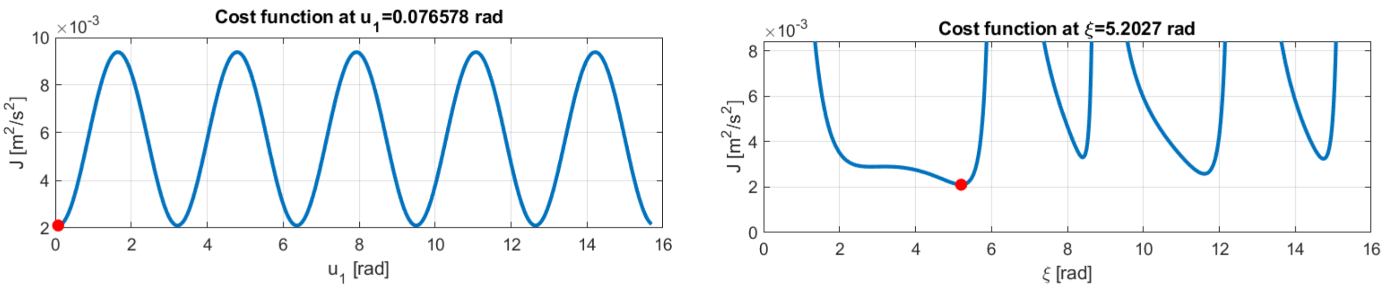

Figure 12: Cost function of scheme №10 solving E1

Lastly, the plot of the function $f(u_2)$ used by scheme №13 is presented. For this particular reconfiguration $|\tilde{Q}|$ happens to be small enough that more than one zeros are found. The chosen $u_2 = 4.6356$ rad minimizes δv_{tot}

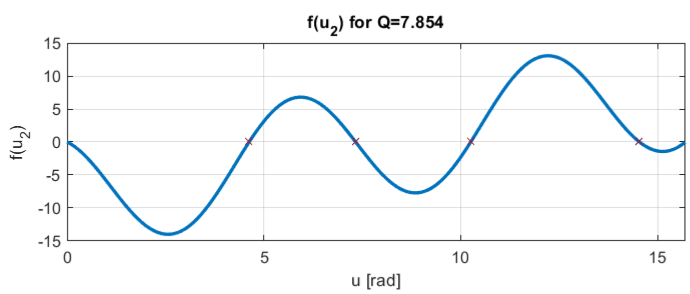

Figure 13: Possible values for u_2 in scheme №13

4.4.2 Problem E2

E2							
$a\delta\boldsymbol{\alpha}_0$ $[m]$				$a\delta\boldsymbol{\alpha}_F$ $[m]$			
50	-10000	230	-50	0	-9800	150	0

Problem E2 is solved also by schemes №3, №9 and №11, for which is necessary a non null variation of relative semi-major axis $A \neq 0$ The less expensive solution is given by scheme №13, but the total delta-v is still greater than the lower bound, which for E2 amounts to $LB_{E2} = 0.0496$ m/s.

₦	u_1	u_2	u_3	δv_{R1}	δv_{T1}	δv_{R2}	δv_{T2}	δv_{R3}	δv_{T3}	δv_{tot}
-	rad			m/s						
3	5.1180	10.4547	-	0	-0.0645	0	0.0382	-	-	0.1027
9	5.4458	8.5874	-	-0.1206	-0.0370	-0.1479	0.0107	-	-	0.2744
11	0	9.4040	-	-0.0215	-0.0343	-0.0307	0.008	-	-	0.0722
12	2.5830	5.7246	15.1494	0	-0.0088	0	-0.0379	0	0.0205	0.0672
13	0	5.2906	15.7080	0	-0.0099	0	-0.0314	0	0.0150	0.0563

Table 3: Problem E2 and solutions

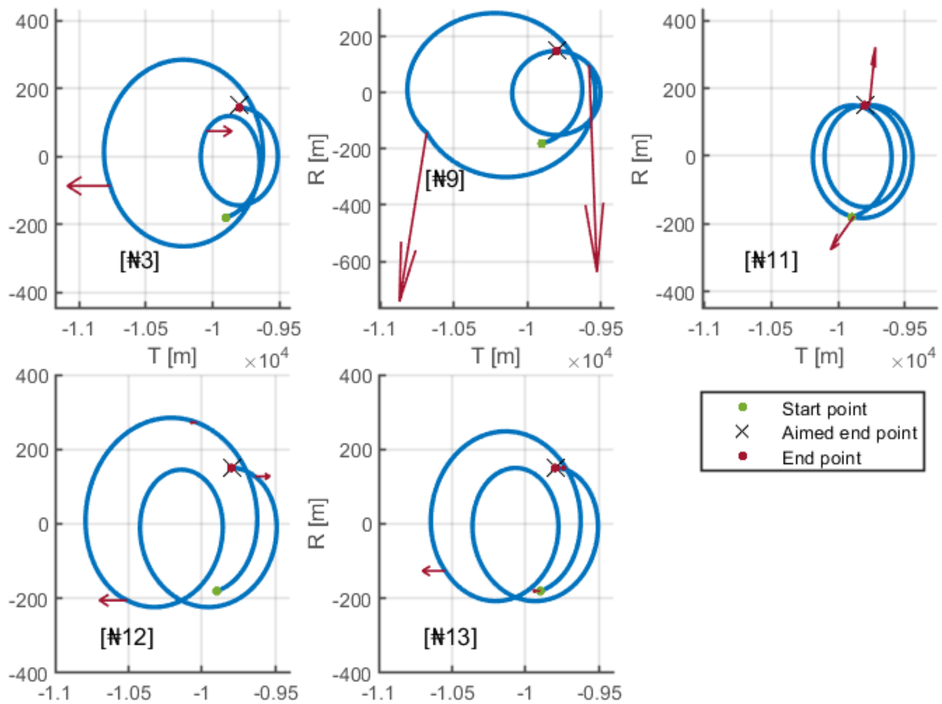

Figure 14: Relative orbits in reconfiguration E2

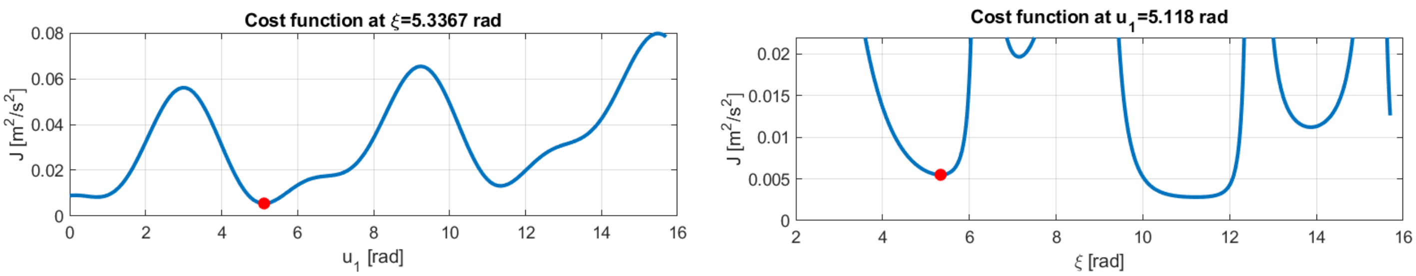

Figure 15: Cost function scheme №3

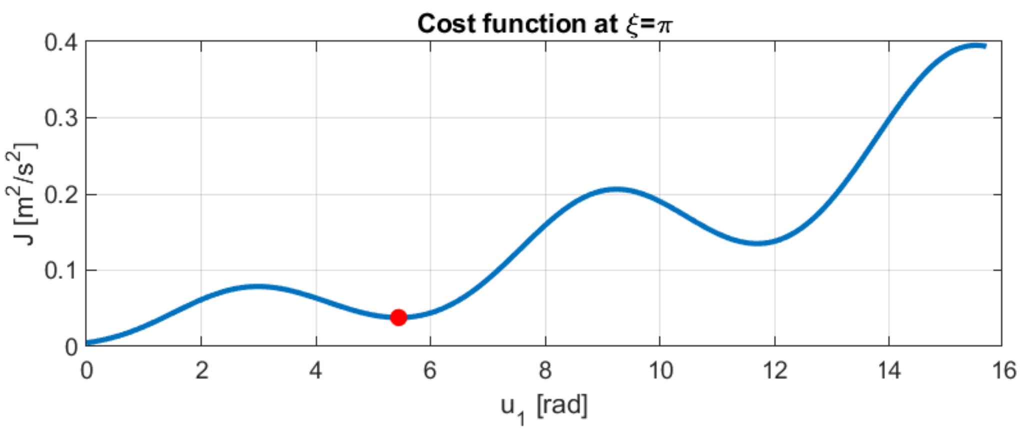

Figure 16: Cost function scheme №9

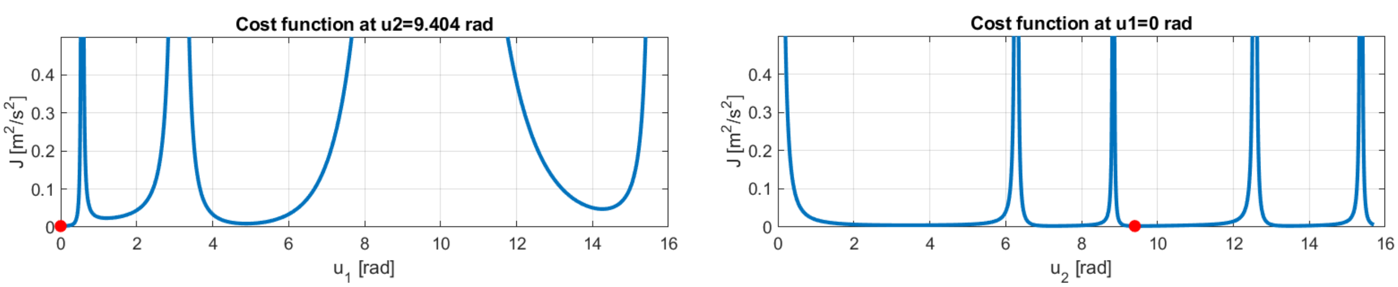

Figure 17: Cost function scheme №11

The delta-v lower bound is is met with solution №12 and an allowed time span of 7.5 orbital periods

№12 Solving E2, $u_F = 15\pi$

u_1	u_2	u_3	δv_{R1}	δv_{T1}	δv_{R2}	δv_{T2}	δv_{R3}	δv_{T3}	δv_{tot}
	rad					m/s			
5.7246	40.2821	43.4237	0	-0.0331	0	0.0116	0	-0.0048	0.0496

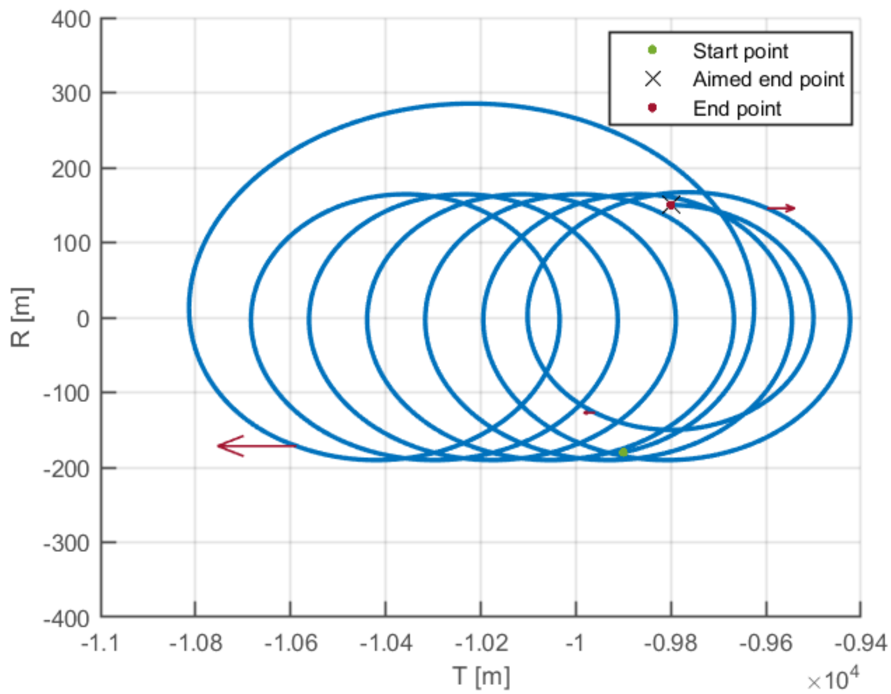

Figure 18: Relative orbit №12 solving E2, $u_F = 15\pi$

4.5 Out-of-plane reconfiguration

The out-of-plane reconfiguration can be solved by two equations in Eq.(15) with unknowns u_M and δv_N:

$$\begin{cases} na\Delta\delta i_x = \cos u_M \delta v_N \\ na\Delta\delta i_y = \sin u_M \delta v_N \end{cases} \tag{19}$$

The change in the inclination vector $\Delta\delta\boldsymbol{i}$ can then be achieved by the following delta-v at latitude u_M:

$$u_M = \arctan\left(\frac{\Delta\delta i_y}{\Delta\delta i_x}\right) + k\pi, \quad \delta v_N = na\|\Delta\delta\boldsymbol{i}\|$$

This formulation doesn't account for the J_2 perturbation described by the state transition matrix, leading to errors on the final state. According to the $\boldsymbol{\Phi}_{J2}$ matrix in Eq.[13] the element δi_y will drift linearly with time and proportionally to δi_x. To account for orbital perturbations the procedure described on [13] can be followed. First the equations for a single delta-v reconfiguration are written:

$$\boldsymbol{\Phi}_{F,1}\boldsymbol{B_1}\delta v = \delta\boldsymbol{\alpha}_F - \boldsymbol{\Phi}_{F,0}\delta\boldsymbol{\alpha}_0 = \Delta\delta\tilde{\boldsymbol{\alpha}}$$

The two equations regarding the out-of-plane dynamics are the following:

$$\begin{cases} \cos u_M \delta v_N = n\Delta\delta\tilde{\alpha}_3 = n\Delta\delta\tilde{i}_x \\ \left[\frac{1}{n}\lambda_I(u_F - u_M)\cos u_M + \sin u_M\right]\delta v_N = n\Delta\delta\tilde{\alpha}_4 = n\Delta\delta\tilde{i}_y \end{cases} \tag{20}$$

Where $\lambda_I = 3n\gamma\sin^2 i$. By dividing the second equation of this system by the first one a transcendental function of the delta-v latitude is found, which has to be solved numerically:

$$\frac{1}{n}\lambda_I(u_F - u_M) + \tan(u_M) = \frac{\Delta\delta\tilde{i}_y}{\Delta\delta\tilde{i}_x}$$

Then the first equation in the system can be used to compute the delta-v magnitude as:

$$\delta v_N = n\frac{\Delta\delta\tilde{i}_x}{\cos u_M}$$

The two maneuvers can be compared by applying them to the following problem: the chief satellite lies on a circular orbit of semi-major axis $a = 6828$ km and inclination $i = 78°$. The initial and final relative orbital elements of the chief-deputy formation are the following, where only the relative inclination vector is non-zero and has to be varied:

$$a\delta \boldsymbol{i}_0 = (10, 70)\ m$$
$$a\delta \boldsymbol{i}_F = (400, 120)\ m$$
$$(a\Delta\delta\tilde{i}_x, a\Delta\delta\tilde{i}_y) = (390, 49.405)\ m$$

The reconfiguration has to be achieved in a time span of seven orbits, meaning $\Delta u = 14\pi$.

Equations	$\delta i_{x,f}$ [m]	$\delta i_{y,f}$ [m]	u_m [rad]	δv_N [m/s]
19	400	143.14	0.126	0.4399
20	400	120	0.0672	0.4374

Table 4: Out of plane maneuvers' comparison

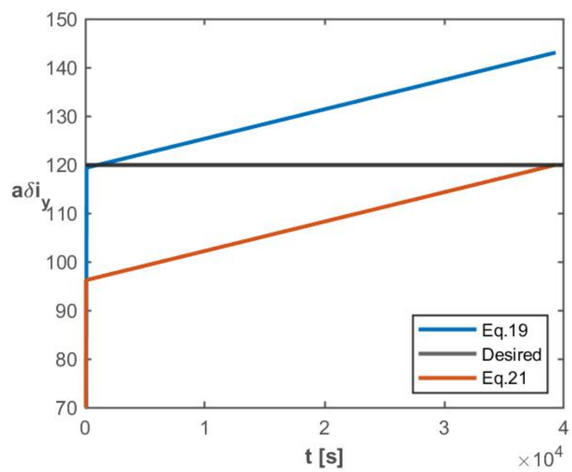

Figure 19: Relative inclination vector's second component variation following the two approaches

It is clear how the first maneuver described by Eq.(19) corrects δi_y to the desired value, but without accounting for the J_2 perturbation that will make it drift from it during the following seven orbits. On the other hand, Eq.(20) gives a slightly different value of u_M and δv_N that alter the ROE of interest so that it will match the desired value at the final time. δi_x is not affected by the J_2 perturbation and will be corrected to the desired value by both approaches

4.5.1 Combined maneuver

The combined maneuver involves one or more impulses with both in plane and out of plane thrust components. The combined maneuver is less expensive than the separated one when the normal impulse required to correct the relative inclination vector should be located at the same mean latitude of one of the in plane impulses. This particular relative inclination vector can be found from Eq.(20) with the following approximation:

$$\frac{\Delta\delta i_y}{\Delta\delta i_x} \approx \frac{\lambda_I}{n}(u_F - u_t) + \tan(u_t) \tag{21}$$

This expression is an approximation because the left hand side term should be equal to $\frac{\Delta\delta\tilde{i}_y}{\Delta\delta\tilde{i}_x}$, which would involve the state transition matrix terms and longer computations. By choosing E2 as in-plane reference problem and a starting relative inclination vector $a\delta\boldsymbol{i}_0 = (\delta i_x, \delta i_y)_0^T = (0,0)^T$ it is found $a\delta\boldsymbol{i}_F = (50, -31.75)^T$. The normal deltav required to accomplish the out of plane reconfiguration would be executed at $u = 2.5615$, while the in plane problem E2 solved with scheme N12 requires a first impulse at $u = 2.5643$, showing that the approximation used is accurate enough.

Taking E1 as in-plane reference problem the procedure is the same: by imposing $a\delta\boldsymbol{i}_0$ with null components it is found by using Eq.(21) $a\delta\boldsymbol{i}_F = (50, 103.095)^T$. The out of plane maneuver would then require a normal impulse at $u = 1.11$ rad, but the first tangential pulse that solves E1 with scheme N12 is located at $u = 4.2581$ rad. This difference arises from the apparently periodic behavior of the second equation of Eq.(20), which has more than one zero. By imposing the normal impulse at $u = 4.2581$ rad the reconfiguration is achieved with a combined deltav 5.466% smaller than the separated one.

	$a\delta\boldsymbol{\alpha}_0$ $[m]$						$a\delta\boldsymbol{\alpha}_F$ $[m]$					
E1	0	-10000	0	0	200	-10	0	-10000	50	103	230	50
E2	50	-10000	0	0	230	-50	0	-9800	50	-31.75	150	0

Table 5: New three dimensional problems

The combined maneuver requires an overall deltav 5.47% smaller than the separated maneuver in E1 and 6.07% smaller in E2.

u_1	u_2	u_3	δv_{T1}	δv_{N1}	δv_{T2}	δv_{N2}	δv_{T3}	δv_{N3}	δv_{comb}	δv_{sep}
rad			m/s							
4.2581	7.3996	10.5412	-0.009	-0.1197	0.018	0	-0.009	0	0.147	0.1555
2.5643	5.7059	15.1307	-0.0085	-0.0632	-0.0381	0	0.0203	0	0.1222	0.1301

Table 6: Three dimensional problems' solutions

4.6 Combined Maneuvers - Parametric studies

The purpose of this chapter is to show a parametric study where reconfigurations with different variations of inclination, longitude of ascending node and argument of periapsis $\Delta i, \Delta\Omega, \Delta\omega$ of the deputy spacecraft's orbit are solved in two different ways. The first one called the T solution solves the in-plane problem with scheme№12 and the out of plane one through Eq.(20). The second one, called RT solution solves the three dimensional problem with a combined maneuver. The first attempt of combined maneuver has been shown in the previous section of this document: given an out of plane problem represented by a variation of the relative inclination vector $\delta\boldsymbol{i}$, an in plane problem $[A, L, E, F]$ was found such that $u_N = u_T$.

In these parametric studies, chief and deputy's initial orbits will be defined by their classical orbital elements $\boldsymbol{\alpha}_c, \boldsymbol{\alpha}_d$, and the initial relative elements $\delta\boldsymbol{\alpha}_0$ of the formation will be computed. Then, deputy's semi-major axis, eccentricity and mean latitude variations $\Delta a, \Delta e, \Delta u$ will be fixed for the three analysis. Regarding the last three elements i, Ω or ω, their variations' values will be fixed two at a time according to Table 7, while the remaining element variations are defined by Eq.(22)

$\boldsymbol{\alpha}$	Chief	Deputy	$\Delta\boldsymbol{\alpha}$	Deputy
a[km]	7000	7010	Δa	-0.05
e	0	0.05	Δe	-0.01
i	45°	44.5°	Δi	0.5°
Ω	0	0	$\Delta\Omega$	0.2°
ω	0	0	$\Delta\omega$	1°
u_0	0	0	Δu	0°

Table 7: Starting orbital parameters

$$\begin{aligned} \Delta\Omega &= 0, 0.2°, \ldots, 1° \\ \Delta i &= 0, 0.2°, \ldots, 1° \\ \Delta\omega &= 1°, 2°, \ldots, 5° \end{aligned} \tag{22}$$

The reconfigurations has to occur in 2.5 orbital periods. RT solution computes the maneuvers as follows:

1. Scheme №12 will solve the in-plane problem, providing the three tangential impulses magnitudes $\delta\boldsymbol{v}_T$ and their mean latitude arguments $\boldsymbol{u}_T$

2. The problem Eq.(20) is solved to find $\delta\boldsymbol{v}_N$ and u_N
3. The closest element of $\boldsymbol{u}_T$ to u_N is made equal to u_N. This means that one of the in-plane maneuvers will be executed at the same time of the normal one, as to combine them and reduce the total cost.
4. The values of the in-plane delta-vs are computed again by solving Eq.(18), in order to still achieve the in-plane ROEs variations with the new maneuvers' mean argument of latitudes $\boldsymbol{u}_T$

The system of equations at Eq.(18) is overdetermined, having three unknowns and four equations. The solutions found by using $\boldsymbol{u}_T = \bar{u} + k_i\pi$ as in scheme №12 always led to the desired in-plane ROEs variations. By changing $\boldsymbol{u}_T$ according to the out of plane problem, no acceptable solutions are found, meaning the final ROEs errors are always big, so the reconfiguration is not achieved.
This problem is overcome by allowing radial maneuvers in the solutions, removing the constraint $x_1 = x_3 = x_5 = 0$. This means that the system will be underdetermined with two degrees of freedom, having now 6 unknowns (three tangential and three radial delta-v values) but still four equations.

4.6.1 Longitude of ascending node variations

The longitude of the deputy's orbit ascending node will be varied from 0 to 1°with variations of 0.2°. The following table shows the in-plane, out of plane and total delta-v calculated by T and RT solutions for every value of $\Delta\Omega_d$. Since increasing $\Delta\Omega$ increases the

	T			RT				
$\Delta\Omega[°]$	δv_{ip}	δv_{oop}	δv_{tot}	δv_{ip}	δv_{oop}	δv_{tot}	In plane red.%	total red.%
0	45.24	65.85	111.09	45.13	65.85	107.39	0.25	3.33
0.2	47.21	68.33	115.54	38.17	68.33	102.07	19.14	11.66
0.4	49.18	75.47	124.66	39.53	75.48	109.80	19.64	11.92
0.6	51.16	86.13	137.28	41.54	86,13	121.73	18.81	11.33
0.8	53.13	99.16	152.29	43.86	99.17	136.36	17.44	10.46
1	55.10	113.77	168.87	46.32	113.78	152.68	15.94	9.59

Table 8: Delta-v values in m/s and their reductions

magnitude of the final relative inclination vector, the out of plane

delta-v will increase as well. This values will be independent of the in-plane control strategy, so they don't change between the T and RT case. The longitude of ascending node also affects the relative mean longitude $\delta\lambda$, so the in-plane delta-vs will vary as well with $\Delta\Omega$. The two different solutions present different in-plane delta-v values, with the RT one being up to 19.6% cheaper at $\Delta\Omega = 0.4°$. The in-plane delta-v reduction comes from the introduction of one radial burn which is performed with one of the tangential ones. This means lower total delta-v values, up to 11.92%. The total delta-v reduction is affected by the combined normal maneuver as well.
Since δv_N is the same between the two solutions, combining it to an in-plane burn will always result in a reduction of total delta-v. This can be seen from the reconfiguration at $\Delta\Omega = 0$, on the first row of Table 8. The in-plane delta-v reduction amounts to 0.25% in the RT solution, while the reduction of total delta-v amounts to 3.33%. These results can be analyzed in the ROEs space, more specifically in the $\delta\lambda, \delta a$ and $\delta e_x, \delta e_y$ planes. In these plots the initial condition is marked by a green circle, it then evolves through a series of segments in order to reach the red circle, which marks the final condition. Grey segments show ROEs variations due to the natural dynamics (Keplerian motion and J_2 effect) which affects $\delta\lambda$ and δe_y. Black segments show impulsive ROEs variations due to performed maneuvers, Eq.(15) can be recalled to remember that tangential burns don't affect $\delta\lambda$, and radial burns don't affect δa.

The length of the black segments is related to the total mission's cost. In fact, [10] shows how the cumulative delta-v cost associated to the $\delta\boldsymbol{\alpha}_0 \longrightarrow \delta\boldsymbol{\alpha}_F$ reconfiguration can be written as a quadratic function of the ROE corrections not related to the natural dynamics, i.e. related only to the m maneuvers performed:

$$J_{plan} = \sum_{i=1}^{m}(a\Delta\delta a)_i^2 + \sum_{i=1}^{m}(a\Delta\delta\lambda)_i^2 + \sum_{i=1}^{m}(\|a\Delta\delta\boldsymbol{e}\|)_i^2 + \sum_{i=1}^{m}(\|a\Delta\delta\boldsymbol{i}\|)_i^2$$

In the ROEs space this is a metric of distance measuring the length of black segments, so minimizing J_{plan} means connecting $\delta\boldsymbol{\alpha}_0$ to $\delta\boldsymbol{\alpha}_F$ with the minimum path, which represents a minimum path problem. The following pictures show the ROEs evolution in the T and RT solutions for $\Delta\Omega = 0.6°$. Initial and final relative eccentricity vectors are out of phase by just $\Delta\omega = 1°$, so the scale on the δe_y has been dilated by approximately two orders of magnitude in order

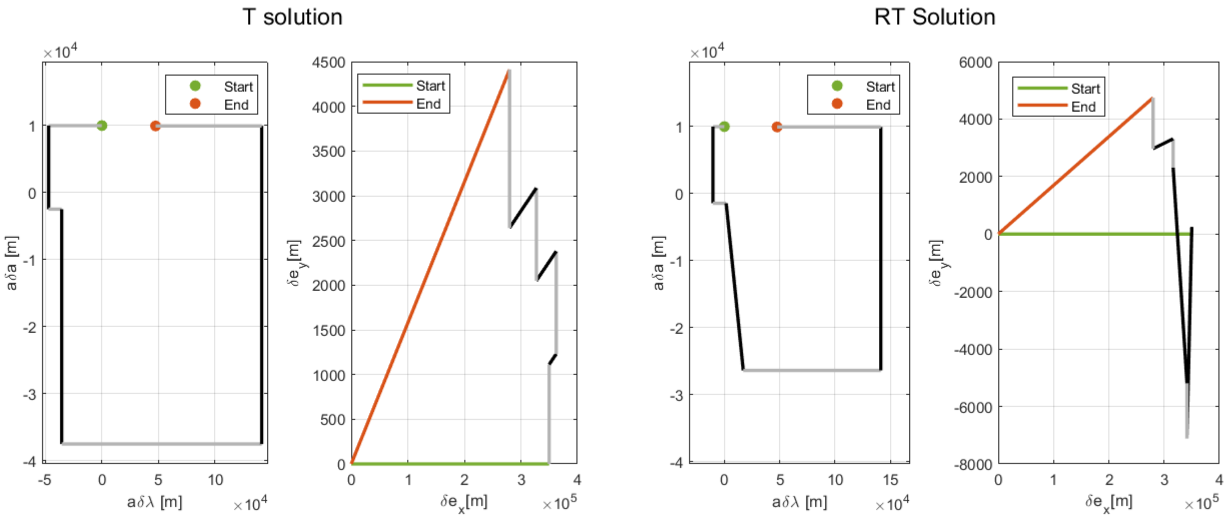

Figure 20: In-plane ROEs variation, $\Delta\Omega = 0.6°$

to distinguish all the different segments. The RT solution biggest difference from the T one lies in smaller δa variations performed by tangential burns, associated to smaller tangential delta-vs. Furthermore, the δe_x variations (larger than the δe_y ones) are all three with the same sign, meaning the delta-v isn't spent to increase that ROE and then decrease it to reach the final aimed state as in the T solution. In this example the introduction of the radial burn allowed to a reduction of in-plane delta-v by 18.8%, and an overall 11.3% delta-v reduction. The following plots summarize the behavior of the various delta-vs as a function of the required RAAN variations.

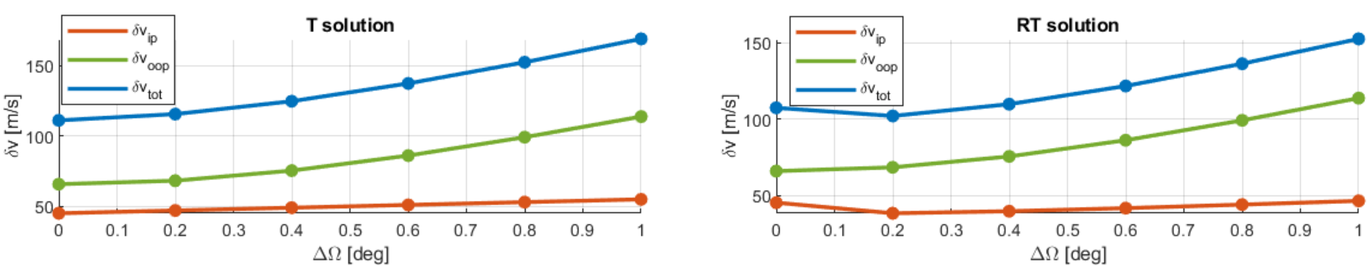

Figure 21: Delta-v values for $\Delta\Omega$ variations

4.6.2 Inclination variations

In this case five formation reconfigurations where the deputy spacecraft's inclination is varied from 0 to 1°with 0.2°steps are solved. All the other COEs variations are fixed by table 7. Table 9 shows how in-plane delta-vs don't change with Δi in the T solution, since scheme №12 solves the in-plane problem without accounting for $\delta \boldsymbol{i}$ variations. This doesn't hold for the RT solution, since in-plane delta-vs are computed again as a function of the normal burn mean argument of latitude u_N. Out of plane delta-vs magnitudes are still equal between the two solutions, and increase as Δi increases.

	T			RT				
$\Delta i[°]$	δv_{ip}	δv_{oop}	δv_{tot}	δv_{ip}	δv_{oop}	δv_{tot}	In plane red.%	total red.%
0	47.21	18.92	66.13	41.59	19.03	59.01	11.92	10.78
0.2	47.21	32.28	79.49	38.53	32.32	67.74	18.39	14.79
0.4	47.21	55.79	103.01	37.98	55.80	89.81	19.56	12.81
0.6	47.21	81.07	128.28	37.84	81.07	114.63	19.85	10.64
0.8	47.21	106.86	154.07	37.79	106.85	140.23	19.95	8.98
1	47.21	132.87	180.08	37.77	132.85	166.14	20.00	7.74

Table 9: Delta-v values and reductions

Again, total delta-v reductions up to 14.8% are shown, as a result of the introduction of a radial burn and the combined normal maneuver, which reduces the in-plane delta-v up to 20%. The following plots on figure 22 show the ROEs evolution for $\Delta i = 0.6°$, with similar differences between the two solutions as noticed in the previous example: impulsive δa variations are smaller in the RT solution, and there are no δe_x variations with different signs between them, while variations of δe_y are still from one to two orders of magnitude smaller.

Finally the delta-v costs as functions of the desired inclination variation are summarized in figure 23.

4.6.3 Periapsis argument variations

Lastly, reconfigurations with different variations of deputy's argument of periapsis ω_d are studied. Their values will range from 0 to 5°, and variations of Ω_d and i_d will be fixed by table 7. This means that only the in-plane ROEs variations $[A, L, E, F]$ will be varied, while $\Delta\delta\boldsymbol{i}$ will be a constant, meaning that δv_N and u_N will be the

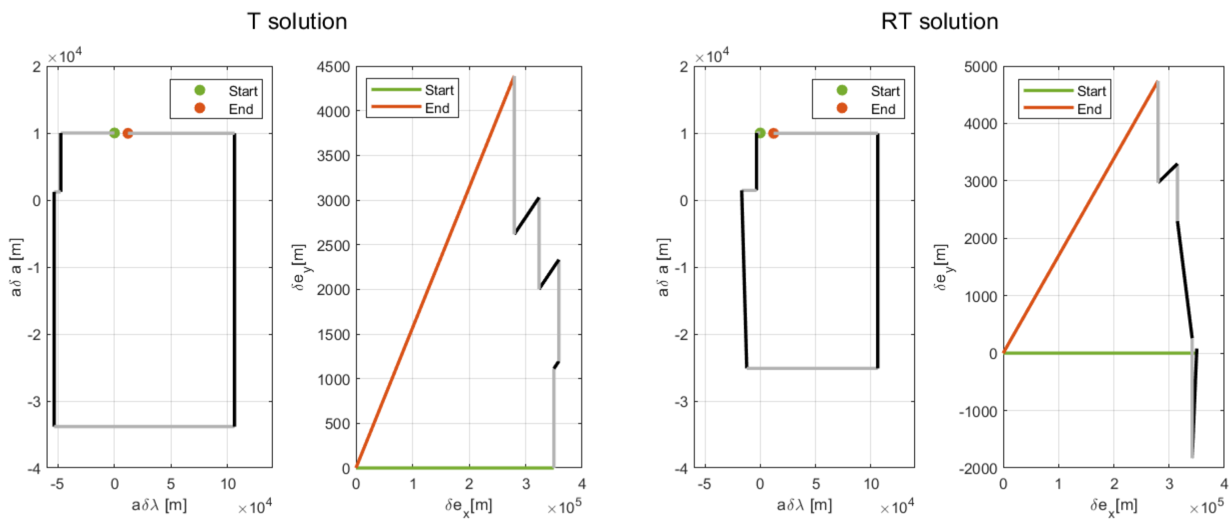

Figure 22: In-plane ROEs variation, $\Delta i = 0.6°$

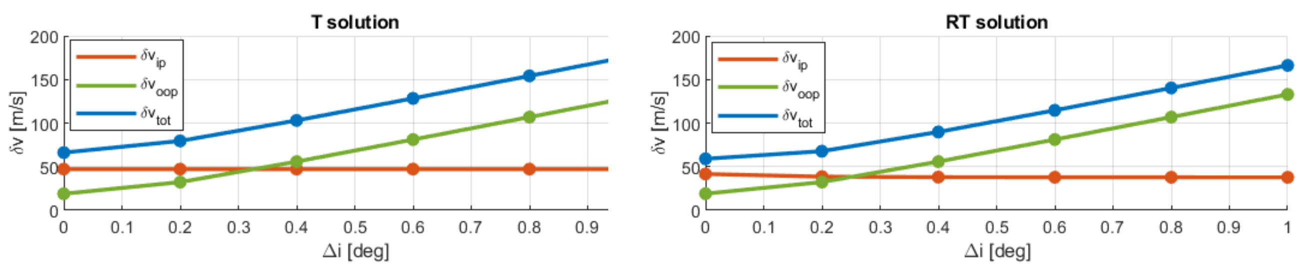

Figure 23: Delta-v values for Δi variations

same for every $\Delta\omega_d$ and in both T and RT solutions. The in-plane total delta-vs computed with the RT solution are now bigger than those obtained with scheme №12 in solution T, for $\Delta\omega > 1°$, with in-plane delta-v increases up to 69%. Combining the normal maneuver with one of the in-plane burns moderates this loss, but the total δv is still approximately 14% bigger in the RT solution.

This phenomenon can be better understood by solving a problem with a much bigger variation of $\Delta\omega = 45°$. This will allow equal scales on both δe_x and δe_y axis, to show the actual length of the path connecting the two vectors in figure 25. The reconfiguration cost is driven by $\delta \boldsymbol{e}$ variations, so in order to achieve an economic enough maneuver, a minimum path traveled by the black segments in this plane will be the priority. This condition is en-

	T			RT				
$\Delta\omega[°]$	δv_{ip}	δv_{oop}	δv_{tot}	δv_{ip}	δv_{oop}	δv_{tot}	In plane red.%	total red.%
0	47.26	68.33	115.59	37.91	68.33	101.97	19.78	11.78
1	47.21	68.33	115.54	37.89	68.33	102.07	19.74	11.66
2	37.87	68.33	106.20	64.01	68.33	121.33	-69.04	-14.25
3	38.23	68.33	106.56	64.02	68.33	121.83	-67.47	-14.33
4	38.81	68.33	107.14	64.44	68.33	122.71	-66.03	-14.53
5	39.61	68.33	107.94	65.25	68.33	123.94	-64.74	-14.83

Table 10: Delta-v values and reductions

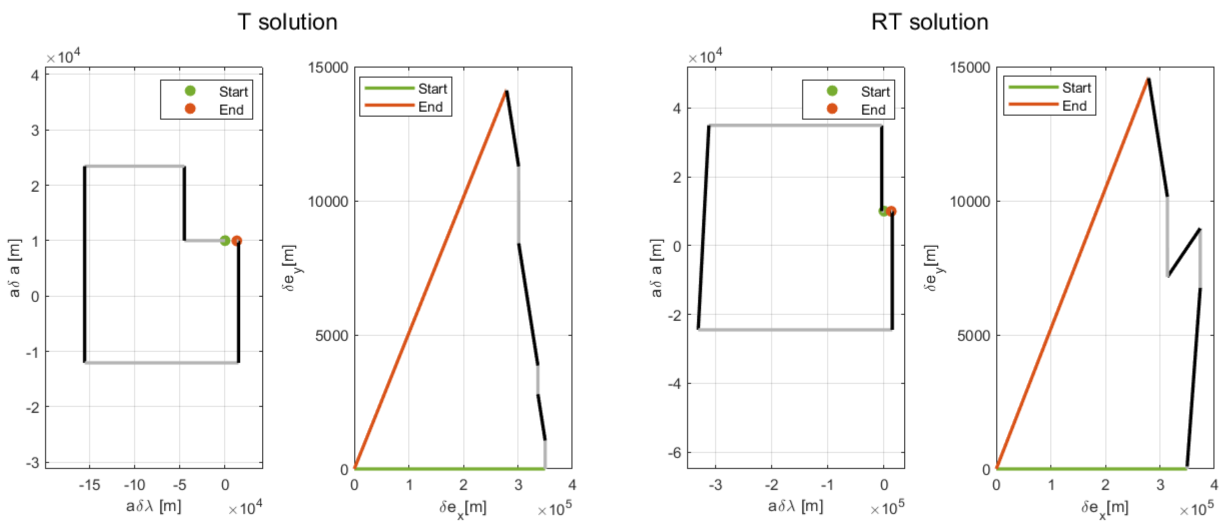

Figure 24: In-plane ROEs variation, $\Delta\omega = 3°$

sured by scheme ₦12, without any radial burns. As remarked by [11], when $\|\Delta\delta\boldsymbol{e}\| > |\Delta\delta a*|$, the absolute minimum cost is achieved whenever the traveled path length in the relative eccentricity vector plane lays parallel to the vector $\delta\boldsymbol{e}_F - \delta\boldsymbol{e}_0$. This happens when all maneuvers occur at some arguments of latitude whose modulus-π equals the one of $\bar{u}$.

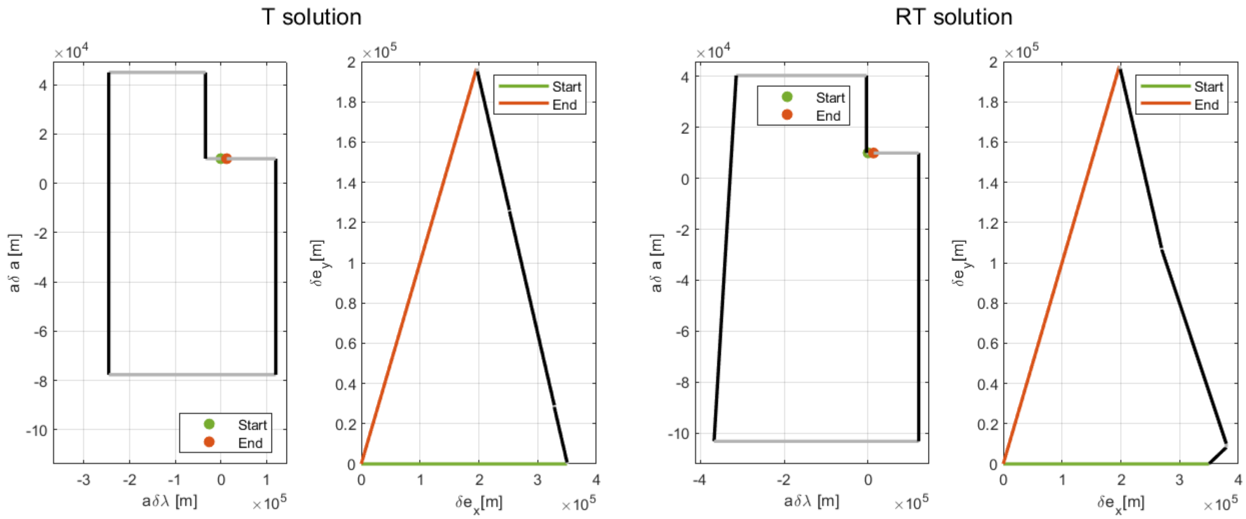

Figure 25: In-plane ROEs variation, $\Delta\omega = 45°$

The minimum path length is shown by the T solution; changing $\boldsymbol{u}_T$ in order to combine the normal burn to one in the orbital plane will result in a longer path, so in a larger overall mission's cost. Moreover, the covered path is longer also in the $\delta\lambda, \delta a$ plane, making the RT solution even less optimal. The in-plane delta-v calculated with the T solution is 16.67% smaller, but a normal burn not combined with an in-plane one makes the overall cost just 6.63% smaller than the RT solution's. Finally, the delta-v values of table 10 are summarized in image 26:

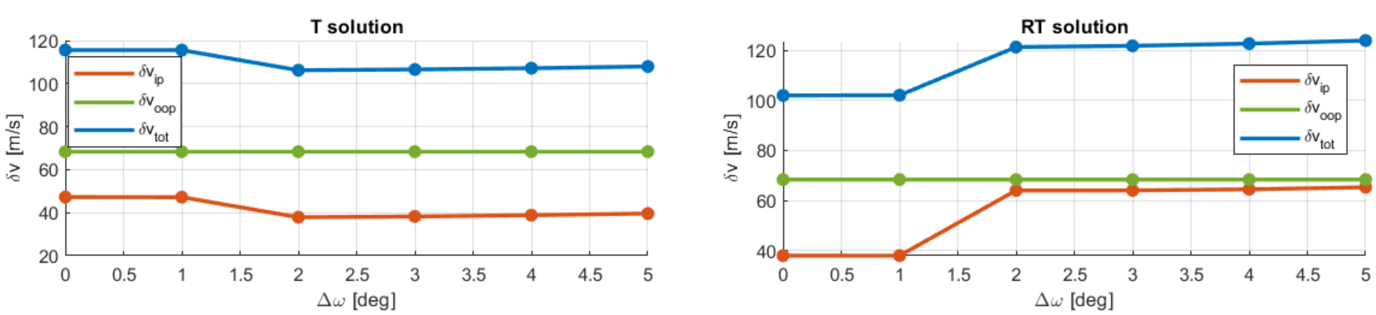

Figure 26: Delta-v values for $\Delta\omega$ variations

5 Conclusion

This thesis showed the mathematical derivation for the state transition matrix needed to compute relative orbital elements variations of a J_2-perturbed satellites formation. Various in-plane maneuvers available in the referenced literature has been tested on two different reconfiguration problems, showing the resulting relative orbits, mission costs and cost function diagrams, highlighting optimal maneuvers.

Out of plane maneuvers has been tested on a different reconfiguration, showing the precaution needed to compensate for J_2 effect on the relative inclination vector

Lastly, a procedure to combine out of plane and in plane maneuver has been developed and applied to reconfigurations with different deputy's COEs variations. Solutions are found by allowing radial burns, which along with the combined normal burns lead to delta-v savings up to 14.8% compared to the separated maneuver. This maneuvering scheme was not always optimal, since for a reconfiguration's cost dominated by $\delta\boldsymbol{e}$ variation, radial burns are less efficient than tangential burns as in scheme №12.

Future works on this topic may investigate how the reconfiguration cost changes with the mission's allowed time span, new models of atmospheric drag and solar pressure disturbances effects on formation flight through state transition matrices, and different maneuvering schemes to compensate for these perturbations' effects on final ROEs of the formation.

References

[1] D.P. Scharf, F.Y. Hadaegh, and S.R. Ploen. "A survey of spacecraft formation flying guidance and control (part 1): guidance". In: *Proceedings of the 2003 American Control Conference, 2003.* Vol. 2. 2003, pp. 1733–1739. DOI: 10.1109/ACC.2003.1239845.

[2] Antoine Labeyrie. "Stellar Interferometry Methods". In: *ARAA* 16 (Nov. 2003), pp. 77–102. DOI: 10.1146/annurev.aa.16.090178.000453.

[3] S. Mathavaraj and Radhakant Padhi. "Introduction and Motivation". In: *Satellite Formation Flying: High Precision Guidance using Optimal and Adaptive Control Techniques.* Singapore: Springer Singapore, 2021, pp. 1–12. ISBN: 978-981-15-9631-5. DOI: 10.1007/978-981-15-9631-5_1. URL: https://doi.org/10.1007/978-981-15-9631-5_1.

[4] Luis Penin et al. "Proba-3: ESA's small satellites precise formation flying mission to study the Sun's inner corona as never before". In: Aug. 2020.

[5] Fred Y. Hadaegh, Soon-Jo Chung, and Harish M. Manohara. "On Development of 100-Gram-Class Spacecraft for Swarm Applications". In: *IEEE Systems Journal* 10.2 (2016), pp. 673–684. DOI: 10.1109/JSYST.2014.2327972.

[6] Howard D.Curtis. *Orbital Mechanics for Engineering Students.* Butterworth-Heinemann, 2011. ISBN: 978-0080971902.

[7] Hanspeter Schaub and John L. Junkins. *Analytical Mechanics of Space Systems.* Amer Inst of Aeronautics and Har/Com, 2003. ISBN: 978-1563475634.

[8] K.F. Wakker. *Fundamentals of astrodynamics.* Institutional Repository. TU Delft Library, 2015. ISBN: 9789461864192.

[9] Montenbruck Oliver et al. "E/I-vector separation for safe switching of the GRACE formation". In: *Aerospace Science and Technology* 10.7 (2006), pp. 628–635. ISSN: 1270-9638. DOI: https://doi.org/10.1016/j.ast.2006.04.001. URL: https://www.sciencedirect.com/science/article/pii/S1270963806000472.

[10] Gabriella Gaias and Jean-Sébastien Ardaens. "Flight Demonstration of Autonomous Noncooperative Rendezvous in Low Earth Orbit". In: *Journal of Guidance, Control, and Dynamics* 41.6 (2018), pp. 1337–1354. DOI: https://doi.org/10.2514/1.G003239. eprint: https://doi.org/10.2514/1.G003239.

[11] Gabriella Gaias, Jean-Sébastien Ardaens, and Oliver Montenbruck. "Model of J_2 perturbed satellite relative motion with time-varying differential drag". In: *Celestial Mechanics and Dynamical Astronomy* 123.10 (2015), pp. 411–433. DOI: https://doi.org/10.1007/s10569-015-9643-2.

[12] G. Gaias and S. D'Amico. "Impulsive Maneuvers for Formation Reconfiguration Using Relative Orbital Elements". In: *Journal of Guidance, Control, and Dynamics* 38.6 (2015), pp. 1036–1049. DOI: 10.2514/1.G000189. eprint: https://doi.org/10.2514/1.G000189. URL: https://doi.org/10.2514/1.G000189.

[13] Michelle Chernick and Simone D'Amico. "New Closed-Form Solutions for Optimal Impulsive Control of Spacecraft Relative Motion". In: *Journal of Guidance, Control, and Dynamics* 41.2 (2018), pp. 301–319. DOI: 10.2514/1.G002848. eprint: https://doi.org/10.2514/1.G002848. URL: https://doi.org/10.2514/1.G002848.